RMetS
Royal Meteorological Society

Representation of daytime moist convection over the semi-arid Tropics by parametrizations used in climate and meteorological models

F. Couvreux,[a]* R. Roehrig,[a] C. Rio,[b] M.-P. Lefebvre,[c] M. Caian,[d] T. Komori,[e,f] S. Derbyshire,[g] F. Guichard,[a] F. Favot,[h] F. D'Andrea,[b] P. Bechtold[e] and P. Gentine[i]

[a]*GMME/MOANA, CNRM-GAME (CNRS and Meteo-France), Toulouse, France*
[b]*LMD, CNRS, Paris, France*
[c]*Meteo-France/LMD, Paris, France*
[d]*SMHI, Norskopping, Sweden*
[e]*ECMWF, Reading, UK*
[f]*Japan Meteorological Agency, Tokyo, Japan*
[g]*Atmospheric Processes and Parametrizations, Met Office, Exeter, UK*
[h]*CRNM-GAME, Toulouse, France*
[i]*Department of Earth and Envrionmental Engineering, Columbia University, New York, NY, USA*

*Correspondence to: F. Couvreux, CNRM-GAME, 42 av G Coriolis, 31057 Toulouse, France. E-mail: fleur.couvreux@meteo.fr

A case of daytime development of deep convection over tropical semi-arid land is used to evaluate the representation of convection in global and regional models. The case is based on observations collected during the African Monsoon Multidisciplinary Analysis (AMMA) field campaign and includes two distinct transition phases, from clear sky to shallow cumulus and from cumulus to deep convection. Different types of models, run with identical initial and boundary conditions, are intercompared: a reference large-eddy simulation (LES), single-column model (SCM) version of four different Earth system models that participated in the Coupled Model Intercomparison Project 5 exercise, the SCM version of the European Centre for Medium-range Weather Forecasts operational forecast model, the SCM version of a mesoscale model and a bulk model. Surface fluxes and radiative heating are prescribed preventing any atmosphere–surface and cloud–radiation coupling in order to simplify the analyses so that it focuses only on convective processes. New physics packages are also evaluated within this framework.

As the LES correctly reproduces the observed growth of the boundary layer, the gradual development of shallow clouds, the initiation of deep convection and the development of cold pools, it provides a basis to evaluate in detail the representation of the diurnal cycle of convection by the other models and to test the hypotheses underlying convective parametrizations. Most SCMs have difficulty in representing the timing of convective initiation and rain intensity, although substantial modifications to boundary-layer and deep-convection parametrizations lead to improvements. The SCMs also fail to represent the mid-level troposphere moistening during the shallow convection phase, which we analyse further. Nevertheless, beyond differences in timing of deep convection, the SCM models reproduce the sensitivity to initial and boundary conditions simulated in the LES regarding boundary-layer characteristics, and often the timing of convection triggering.

Key Words: AMMA field campaign; CMIP5 models; diurnal cycle; parametrization of shallow and deep convection; semi-arid regions; single-column models

Received 10 July 2014; Revised 23 December 2014; Accepted 13 January 2015; Published online in Wiley Online Library

1. Introduction

The diurnal cycle of convection is a dominant mode of variability in the Tropics (Hastenrath, 1995), but its accurate representation still challenges numerical models. Over land in general, and over West Africa in particular, global and regional models tend to simulate the maximum of precipitation a few hours too early and typically in phase with the peak in surface heat

fluxes (Yang and Slingo, 2001; Betts and Jakob, 2002; Dai and Trenberth, 2004; Nikulin *et al.*, 2012; Roehrig *et al.*, 2013; Song *et al.*, 2013). A number of studies highlighted the role of convective parametrizations in shaping the simulated diurnal cycle of convection (Betts and Jakob, 2002; Guichard *et al.*, 2004; Stirling and Stratton, 2012; Bechtold *et al.*, 2014). These studies underlined the typical absence or poor representation of the growing cumulus phase. Progress on the physics of convective parametrizations appears to at least partially correct this deficiency (Rio *et al.*, 2009, 2013; del Genio and Wu, 2010; Stratton and Stirling, 2012), however, the representation of the diurnal cycle of dry and moist convection remains an important issue for climate and weather prediction models (Svensson *et al.*, 2011; Couvreux *et al.*, 2014). Convection displays a well-defined diurnal cycle over land, induced by the small soil thermal inertia, so that assessing its representation in models by comparison with high-resolution models and observations is an attractive methodology for evaluating and improving model physics (Dai and Trenberth, 2004).

Here we present a continental convection case in which the amplitude of the diurnal cycle is large (Dai, 2001; Nesbitt and Zipser, 2003; Medeiros *et al.*, 2005; Gounou *et al.*, 2012). The case study is located in the semi-arid Sahel. Such a semi-arid environment (hot and dry) corresponds to relatively unexplored atmospheric conditions where triggering mechanisms may differ from the humid Tropics or mid-latitudes. In fact, studies of the daytime convection in semi-arid regions are scarce, despite the large portion of continents covered by such an environment. Most studies on the diurnal cycle and the transition from shallow to deep convection have focused on the wet Tropics (Grabowski *et al.*, 2006, G06 in the following; Khairoutdinov and Randall, 2006) or mid-latitudes (Guichard *et al.*, 2004, G04 in the following). The results of the intercomparison will be discussed in relation to these studies in order to highlight the progress in the development of parametrizations that have been achieved in the past 10 years. In the present case study, initiation of convection tends to occur later: the lag between the first shallow clouds and deep clouds is 3–4 h in G04 and G06, whereas it is 5–6 h in the present semi-arid case. Such delay is mainly related to the large convective inhibition (CIN) and associated hot and dry boundary layer.

A large-eddy simulation (LES) set-up has been derived based on, and validated with, observations (Couvreux *et al.*, 2012, C12 in the following). This LES serves as a reference against which different single-column models (SCM) are compared. We focus here on the representation of the convective initiation and the preconditioning of the atmosphere (i.e. modification of thermodynamic mean profiles before convective initiation by processes such as dry and moist turbulence), which is thought to be critical for the diurnal course of continental deep convection (Guichard *et al.*, 2004). A strong surface forcing is highlighted and the large amplitude of the sensible heat flux is the main source of convective initiation, typical of dry and hot environments. A study of the climatology of this type of convection observed at this site also confirms the importance of deep, dry, convective boundary layers (Dione *et al.*, 2014). Surface heterogeneities can also play a significant role in the initiation of deep convection as shown by Taylor *et al.* (2011), but this is not the focus here and surface fluxes are prescribed homogeneously over the domain in the LES.

The objectives of this work are twofold: (i) to investigate the ability of the models to initiate deep convection in semi-arid environments and (ii) to analyse the different processes at play, such as the boundary-layer turbulence and shallow convection, particularly during the transitions from clear sky to shallow cumulus and from shallow to deep convection. We use the same initial and boundary conditions as the LES for the different SCM versions of the models. The SCM is built by extracting a single atmospheric column of a model, which integrates the same suite of subgrid physics (boundary-layer, shallow convection, deep convection and microphysics scheme) as the atmospheric component of the Earth system models (ESMS) but in a constrained large-scale environment. The joint utilization of the LES and SCM is now part of a common methodology (Randall *et al.*, 1996) widely used within the GEWEX Cloud System Study (GCSS; where GEWEX is the Global Energy and Water Cycle Experiment) project (Browning *et al.*, 1993) for the development of parametrizations (Siebesma and Cuijpers, 1995; Hourdin *et al.*, 2013). Betts and Jakob (2002) showed that several major global model deficiencies are reproduced when using a SCM, in particular the misrepresentation of the diurnal cycle of deep convection. The general aim of this article is to assess the physical realism of the parametrizations of dry and moist atmospheric convection used in those SCMs, based on the comparison of the SCM results with the LES that have been validated previously using observations collected during field campaigns (C12). As such, we propose a framework (observation, LES, SCM) to assess the behaviour of the SCM's boundary-layer and shallow- and deep-convection parametrizations. The parametrizations studied here are taken from the Coupled Model Intercomparison Project (CMIP) 5 versions and from more recent versions of the same models.

In the following, section 2 describes the case set-up, the models and the different simulations. The results for the different SCMs are presented in section 3, with a focus on the initiation of deep convection. Section 4 focuses on the preconditioning of the environment before initiation of deep convection, namely the evolution of the boundary layer and the development of shallow cumulus; in particular, different SCMs with the deep convective scheme turned off are compared to the LES. Section 5 presents various sensitivity tests in order to highlight how the models are able to reproduce the sensitivity to initial and boundary conditions simulated by the LES.

2. Case description

The case study investigated here is taken from observations during 10 July 2006 of the African Monsoon Multidisciplinary Analysis (AMMA) field campaign in which a relatively small and short-lived convective system developed over Niamey (Lothon *et al.*, 2011). Even though small, the system involved the development of a few cells during its whole life cycle (about 6 h). This system propagated 300 km to the west of the location of initiation. The whole convective transition was observed by several ground-based instruments (radar, wind profiler and atmospheric soundings) and has been complemented by satellite data. This case study concerns a typical case of transition from shallow to deep convection over semi-arid regions, as frequently observed in the Sahel in late Spring and early Summer before the onset of the monsoon (Dione *et al.*, 2014). It is characterized by a low evaporative fraction and associated with an elevated cloud base and high boundary layer (about 2.5 km). In these situations convection appears to be more likely over a drier surface and is favoured by high surface sensible-heat fluxes (Findell and Eltahir, 2003; Guichard *et al.*, 2009; Taylor *et al.*, 2011). This case was also chosen for the weakness of large-scale synoptic forcing such as African Easterly Waves, which are known to favour deep convection (Burpee, 1974), but appear to have only a minimal impact here.

2.1. Set-up

The set-up is exactly the same for both the SCM simulations and the LES. It is summarized below and more extensively described in C12. Surface sensible- and latent-heat fluxes inferred from observations (Figure 1) are prescribed, while surface friction is parametrized using a prescribed roughness length of 0.01 m. The initial vertical profiles of temperature, moisture and wind, based on an early morning sounding, are shown in Figure 1. Compared with other intercomparison experiments (over the US Southern Great Plains (G04) or the Amazon (G06)), the vertical profile is

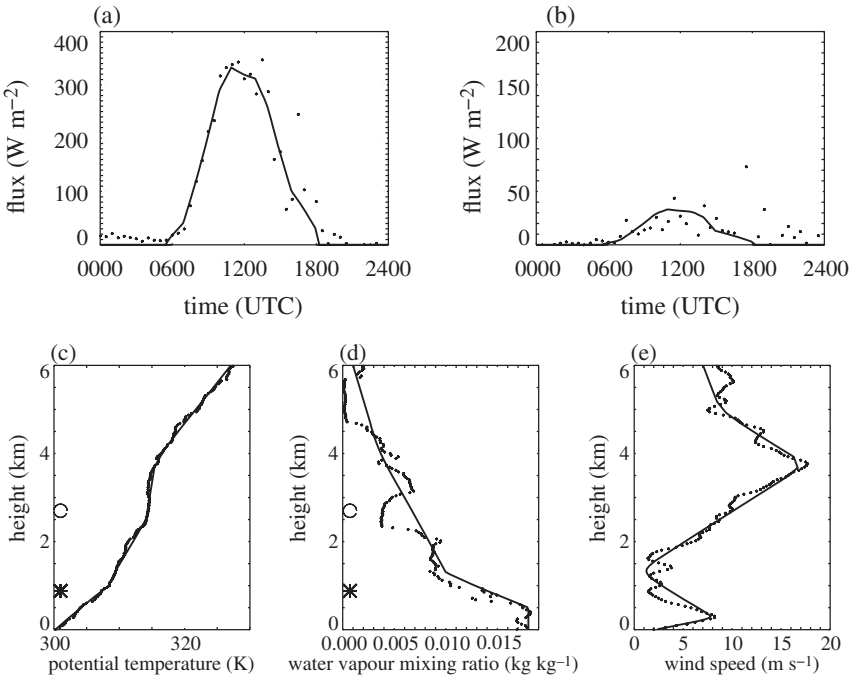

Figure 1. (a) Sensible and (b) latent heat-flux boundary conditions and initial profiles of (c) potential temperature, (d) water-vapour mixing ratio and (e) wind speed for the reference simulation (solid lines). Observations (black dots) are from the Niamey sounding at 0530 UTC and from the ARM flux tower at Niamey airport. The star and the circle indicate, respectively, the lifting condensation level and the level of free convection.

warmer, with a smaller vertical gradient of potential temperature between 1000 and 5000 m. A low-level jet occurs in the early morning (Lothon *et al.*, 2008) but is quickly eroded at sunrise: also note the presence of the African easterly jet, located at about 4000 m above the surface (Figure 1(e)).

Large-scale advection, based on the AMMA European Centre for Medium-range Weather Forecasts (ECMWF) reanalysis (Agusti-Panareda *et al.*, 2010) and observations, is taken into account. The large-scale horizontal advection is composed of cooling (0.3 K h^{-1} maximum) and moistening (0.3 g kg^{-1}h^{-1} maximum) tendencies affecting only the low levels (below 3000 m) in the morning (the maximum is prescribed at 0600 UTC and then linearly decreased down to 0 at noon, see figure 6 of C12). Prescribing those large-scale tendencies in the SCM and LES is a simple but physically based approach to account for the thermodynamic impact of the monsoon flow. A large-scale vertical velocity of 1.5 cm s^{-1} from 1200 to 1800 UTC is prescribed below 5000 m to represent the mesoscale circulation induced by surface heterogeneities. Time-varying profiles of the divergence of radiative fluxes are also prescribed (in the same way as in C12). Here, surface fluxes as well as radiative heating are prescribed preventing any surface–atmosphere and cloud–radiation coupling in order to simplify the analysis and to focus on convective processes. The Coriolis effect is ignored. The simulations start at 0600 UTC and end at 1800 or 2400 UTC depending on the models.

2.2. *The LES reference simulation*

The reference LES has been performed with the MesoNH model (Lafore *et al.*, 1998). In the LES configuration, only small-scale turbulence parametrization is activated with a turbulence kinetic energy (TKE) prognostic scheme (Cuxart *et al.*, 2000) using a length-scale proportional to the grid size. The domain is 100 × 100 km^2 with a horizontal resolution of 200 m: the sensitivity to the resolution has been explored in C12. A vertical stretched grid of 118 levels is used with resolution finer than 50 m in the boundary layer (BL) and up to 2000 m and coarser higher up (reaching 250 m at the top of the model). The lateral boundary conditions are cyclic. In addition to the set-up described above, a random potential temperature perturbation of 0.1 K is added to the horizontally homogeneous initial state at the lowest level in order to initiate turbulent motions. This simulation has been evaluated against numerous observations (radiosondes, radar, satellites, ceilometers) in C12 and correctly reproduces the growth of the boundary layer, the development of shallow cumulus and the initiation of deep convection observed that day.

2.3. *The models*

Different versions (the version used for the CMIP5 runs and newer versions) of four ESMs are evaluated. In addition, two versions of an operational weather forecast system, a mesoscale model and a probabilistic bulk model, participated in this intercomparison. All those models have been run in a SCM configuration. The different models and their parametrizations are summarized in Table 1 and a short presentation of each model is given below.

The atmospheric component of the Centre National de Recherches Météorologiques (CNRM) climate model, ARPEGE-Climat, has been run with three different physics packages: the one used for the CMIP5 experiments (CNRM-CM5, Voldoire *et al.*, 2013) and two other current developments, CNRM-PROG and CNRM-PCMT, that differ essentially in the boundary-layer, convection and microphysics scheme (see Table 1). The CNRM-CM5 uses 31 vertical levels, while the other two use 71 and 91 vertical levels respectively: all use a time step of 300 s.

The ECMWF_IFS model is an operational weather forecast model and has been run with both the physics of the operational version CY38r1, ECMWF-I38, and the physics of the operational version CY40r1, ECMWF-I40, which differ only by a modification of the convection closure (Bechtold *et al.*, 2014). The first version is used with 71 vertical levels and a 60 s time step, while the second uses the operational 137 vertical levels and a 900 s time step.

The EC-Earth climate model has been run with the standard CMIP5 version, EC-Earth-CM5 (Hazeleger *et al.*, 2010), which is based on the CY36r4 version of the ECMWF operational model, a version close to the one used in the ECMWF-I38, with some differences in the cloud scheme and entrainment and detrainment formulations (see next section). The second version, EC-Earth-v2, follows the standard version with some modifications of the boundary-layer and convection schemes. Those runs were performed with 91 vertical levels and a 900 s time-step.

Table 1. The different parametrizations of the different single-column models.

Model (number of vertical levels, time-step)	Boundary layer	Shallow convection	Deep convection	Clouds and microphysics
CNRM-CM5 (31, 300 s)	Diagnostic TKE (Ricard and Royer, 1993), non-local mixing length (Lendering and Holtslag, 2004)	No specific scheme, handled by turbulence scheme	Mass-flux scheme (Bougeault, 1985); triggering depends on moisture convergence and stability profile; fixed profile of ε; δ deduced from moist static energy conservation; no downdrafts	Exponential/Gaussian law of the saturation deficit (Bougeault, 1982)
CNRM-PCMT (91, 300 s)	Prognostic TKE, non-local mixing length (Cuxart *et al.*, 2000) + mass-flux component (Guérémy, 2011)	Same scheme as deep = unified scheme	Piriou *et al.* (2007) and Guérémy (2011) prognostic equation of w_u; CAPE closure ($T = 3$ h); $\varepsilon = \varepsilon_t + \varepsilon_o$; ε_t: buoyancy sorting	Triangular law for clouds (Smith, 1990), prognostic microphysics for the convection and large scale (Lopez, 2002)
CNRM-PROG (71, 300 s)	As CNRM-PCMT without the mass-flux component	Mass-flux scheme (Bechtold *et al.*, 2001) parcel triggering	As CNRM-CM5 + condition on cloud depth >3 km	Prognostic LS cloud water and precipitation (Lopez, 2002)
ECMWF-I r38 (71, 60 s)	Dual EDMF (Köhler *et al.*, 2011), non-local K profile	Bulk mass-flux scheme (Tiedtke, 1989) closure from a balance assumption for the subcloud layer	Bulk mass-flux scheme (Tiedtke, 1989) CAPE closure parcel triggering The turbulent ε and δ depends on relative humidity	Prognostic cloud, condensate and precipitation (Tiedtke, 1993; Forbes *et al.*, 2011)
ECMWF-I r40 (137, 900 s)	As ECMWF-I r38	As ECMWF-I r38	Modification of convection closure described in Bechtold *et al.* (2014)	As ECMWF-I r38
EC-EARTH-CM5 (91, 300/900/1800 s)	As ECMWF_Ir38	As ECMWF_Ir38	As ECMWF_Ir38 but different lateral exchange rates $\varepsilon = \varepsilon_t(R_{up}, R_h)$ $\delta = \delta_t + \delta_o(\mathrm{d}w_u/\mathrm{d}z)$	As ECMWF-I r38
EC-EARTH-v2 (91, 300 s)	Modification of the diffusion part: top entrainment from surface scaled by the boundary-layer height	As EC-Earth	Modification of ε (rescaling in the first-guess and full updraught computations)	As EC-Earth
HadGEM-CM5 (38, 600 s)	K-theory + non-local terms (no mass-flux scheme)	As deep convection, but modified after Grant and Brown (1999)	Mass-flux scheme (Gregory and Rowntree, 1990), CAPE closure, adaptive δ (Derbyshire *et al.*, 2011)	Diagnostic cloud (Smith, 1990)
HadGEM-v2 (70, 600 s)	As HadGEM-CM5	As HadGEM-CM5	As HadGEM-CM5	Prognostic cloud and condensate (PC2; Wilson *et al.*, 2008)
LMDZ5A (39, 450 s)	Diffusivity = $f(Ri\_\mathrm{local})$ countergradient = 1 K km^{-1}	No explicit scheme but handled by Emmanuel scheme	Emanuel (1993): saturated and unsaturated downdrafts ε,δ = buoyancy sorting CAPE closure	Log-normal law (Bony and Emanuel, 2001) for clouds, Sundquist scheme for precipitation
LMDZ5B (39, 450/60 s)	Prognostic TKE scheme (Mellor and Yamada, 1974) + mass-flux scheme (Rio and Hourdin, 2008)	Mass-flux scheme from ground (Rio and Hourdin, 2008; Rio *et al.*, 2010)	Emanuel (93) + cold pools + available lifting energy/availalbe lifting power (Grandpeix and Lafore, 2010)	Log-normal for LS clouds and bi-Gaussian law for shallow clouds (Jam *et al.*, 2013) as LMDZ5A for precipitation
LMDZ5S (39, 450 s)	Same as LMDZ5B	Same as LMDZ5B	Stochastic triggering (Rochetin *et al.*, 2014)	Same as LMDZ5B
MNH (116, 120 s)	Mass-flux scheme (Pergaud *et al.*, 2009) + tke prognostic scheme as CNRM-PROG	Mass-flux scheme (Pergaud *et al.*, 2009)	Mass-flux scheme (Bechtold *et al.*, 2001) Parcel triggering → depth criteria CAPE closure	As CNRM-CM5 for LS clouds, directly derived from the mass-flux scheme for shallow clouds. Kessler scheme for precipitation (Pinty and Jabouille, 1998)
PPM (6 layers, 60 s)	Semi-analytical, from pdf of surface plumes characteristics. ε = constant = $f(h)$ Gentine *et al.* (2013a)	Entraining plume model. $\varepsilon = f(z)$ and δ to impose a decreasing Mf from De Rooy and Siebesma (2008) and Gentine *et al.* (2013c)	Same as shallow convection. As soon as precipitation is initiated, ε is reduced based on the cloud size (D'Andrea *et al.*, 2014)	Cloud fraction computed as the probability of active plumes; simple precipitation parametrization (D'Andrea *et al.*, 2014)

TKE, turbulent kinetic energy; LS, large scale; ε and δ entrainment and detrainment rate; ε_t/δ_t ε_o/δ_o, turbulent and organized entrainment/detrainment rates; w_u, vertical velocity of the updraught; Mf, mass flux.

The UK Met Office HadGEM climate model has been run with two different physics configurations: the standard CMIP5 version, HadGEM-CM5 (based on the HadGEM2-A climate model, Jones *et al.*, 2011; Martin *et al.*, 2011) and the GA4 version, HadGEM-v2 (based on the HadGEM3 climate model), which includes a prognostic cloud and condensate scheme (Wilson *et al.*, 2008). They also vary in terms of vertical resolution, with 38 levels for the HadGEM-CM5 and 70 for HadGEM-v2, but both use a 600 s time step.

The Institut Pierre Simon Laplace (IPSL) climate model has been run with three different physics packages, corresponding to the two versions available in the CMIP5 archive plus a newer version. They have been run with 39 vertical levels and a 450 s time-step. The first physics package, LMDZ5A used in IPSL-CM5A (Dufresne *et al.*, 2013), is close to the version previously used in the CMIP3. The second physics package, LMDZ5B used in IPSL-CM5B, has been completely revisited, with modifications to the representation of the boundary-layer turbulence and how it is coupled to the convection scheme (Hourdin *et al.*, 2013). The LMDZ5S (for LMDZ5 stochastic) uses the same physics package as the LMDZ5B, but with a modification of the triggering of deep convection that takes into account a spectrum of thermal sizes (Rochetin *et al.*, 2014a, 2014b).

The Meso-NH model can be run for a large range of resolutions, from a very fine grid (a few metres) to a large grid (several tens of kilometres). In addition to the LES configuration adopted as a reference in this work, it is also used in its SCM version (with turbulence, thermal and shallow cumulus and deep convection parametrizations activated; see Table 1) with the same vertical resolution as the LES and a time step of 120 s. In the following 'MNH' refers to this SCM simulation.

The Probabilistic Plume Model (PPM) is a bulk model (Gentine *et al.*, 2013a, 2013b; D'Andrea *et al.*, 2014) in which the vertical resolution is not explicit, but it uses up to six different layers with evolving thickness and the time step is 60 s.

Note that several results presented hereafter should also be relevant for other models, in particular regional models that use the same type of parametrizations (Nikulin *et al.*, 2012).

Each model has been run with its native vertical grid and time step (Table 1). Figure A1 shows the vertical grid of the different models. The LMDZ versions, HadGEM-CM5 and CNRM-CM5 use the coarsest resolution, in particular in the boundary layer, with a vertical resolution larger than 200 m above 300 m for the LMDZ versions, above 500 m for the HadGEM-CM5 and above 700 m for the CNRM-CM5. Two sets of runs have been carried out where modifications of the set-up have been tested, either with a small amplitude for ensemble runs (described in the Appendix) in order to assess the robustness of the results, or with a larger amplitude for sensitivity tests that are described in section 5.

3. Timing and intensity of deep convection

In this section, we present the timing and intensity of deep convection in the different SCMs. We first detail the differences among the various deep convection parametrizations. We then discuss the results and evaluate the relevance of the triggering criteria of several schemes using the LES.

3.1. Similarities and differences in the formulation of deep convection in models

All the deep convection schemes of this study are based on a mass-flux approach. They differ, however, in the details of the triggering and closure (which controls the intensity of convection) and in the formulation of lateral exchanges with the environment (entrainment and detrainment rates), as described below.

3.1.1. Triggering criteria

All the deep convective schemes studied here use a triggering based on a parcel diagnosis, but they use a different lifting hypothesis (with or without entrainment) and different thresholds for the triggering criterion. In the LMDZ5A, MNH and HadGEM, the triggering of the deep convection scheme is determined by comparison of the buoyancy of a lifted parcel with a given threshold. In both versions of the EC-Earth and ECMWF, a criterion on the depth of the cloud is added. A criterion based on large-scale moisture convergence and stability is used for the CNRM-CM5 and CNRM-PROG (Bougeault, 1985), with an additional condition on the cloud thickness for the CNRM-PROG. An available lifting energy (ALE) from subcloud processes (Grandpeix and Lafore, 2010) is used for triggering in the LMDZ5B. This energy is the sum of the maximum energy produced by the thermals and by the cold pools generated by the evaporation of precipitation under convective systems. It must be greater than the CIN to trigger deep convection. In the LMDZ5S, this triggering is modified to take into account a spectrum of thermal sizes in the boundary layer, leading to an additional stochastic condition (Rochetin *et al.*, 2014a, 2014b). There is no triggering concept in the CNRM-PCMT and PPM as those schemes involve a prognostic equation of the updraught vertical velocity.

3.1.2. Closure

Most of the deep convection schemes use a convective available potential energy (CAPE) closure with different relaxation timescales. In both versions of the EC-Earth, in the ECMWF and in the CNRM-PCMT, the relaxation time depends on the cloud depth and updraft vertical velocity. In HadGEM, this time is a function of relative humidity. In the LMDZ5A and MNH, the relaxation time is fixed to 2 h 15 min and 1 h respectively. In the ECMWF-I40, the closure is dependent on an extended CAPE based on a quasi-equilibrium assumption for the free troposphere subject to boundary-layer forcing (Bechtold *et al.*, 2014). Several models use a different type of closure: the CNRM-CM5 and CNRM-PROG use a Kuo-type closure based on a moisture budget; in the LMDZ5B, the closure is a function of the available lifting power (ALP) computed using thermal and cold-pool properties (Grandpeix and Lafore, 2010) as well as the CIN and a vertical velocity dependent on the level of free convection (Rio *et al.*, 2013); in the PPM, the mass flux is based on the integration of the vertical velocity across all plumes reaching the level of free convection.

3.1.3. Entrainment and detrainment rates

Two typical formulations are used in the different convective schemes for the lateral entrainment (ε) and detrainment (δ) rates (Table 1). The first type of formulation uses a prescribed profile depending on the altitude only, as in the CNRM-CM5 and CNRM-PROG, and/or physical parameters such as the relative humidity, as in the ECMWF. The second type of formulation is based on a buoyancy-sorting formulation (Bechtold *et al.*, 2001), such as in all versions of the LMDZ and in the MNH. Some models use a mixture of both formulations, as in the CNRM-PCMT, in both versions of the EC-Earth and in the HadGEM. In PPM, on top of a simplified lateral buoyancy-sorting formulation (De Rooy and Siebesma, 2010), ε is rescaled by the depth of the cloud as soon as precipitation reaches the ground.

In the following, we examine the impact of the combination of triggering, closure and entrainment/detrainment formulations on the timing and initiation of deep convection, in particular: comparison of the LMDZ5B and LMDZ5S, which differ only in their triggering function, will assess the impact of the triggering function; comparison of the two versions of the ECMWF, which differ only in their closure, will assess the impact of the closure; and comparison of both versions of the EC-Earth, which differ mainly in their entrainment rates, will assess the impact of the formulation of entrainment rates.

3.2. Results

In the LES, deep convection initiates around 1645 UTC and surface precipitation starts at 1700 UTC but remains at a relatively small intensity, reaching 7 mm day^{-1} at 1800 UTC (Figure 2). The warming (up to 1.2 K h^{-1}) of the levels above 3 km starts at 1700 UTC, associated with a cooling (up to 0.5 K h^{-1}) and drying (up to 0.3 g kg^{-1}h^{-1}) of the boundary layer due to the combined effect of unsaturated downdraughts and evaporation of precipitation (Figures 3 and 4). A net moistening of the mid-tropospheric levels is observed from 1000 to 1800 UTC and is due to the transport and detrainment of moisture by the boundary-layer convection, the shallow clouds and the deep convection, whereas the heat transport induces a cooling of the mid-levels before initiation of deep convection, which is then counterbalanced by the water phase change (formation of hydrometeors) and the compensating subsidence inducing a significant warming only after 1700 UTC.

Across the SCMs, the time evolution of the precipitation, shown in Figure 2(a,b), indicates a large spread in the onset time of the first rain and also in surface precipitation intensity. The common bias in the diurnal cycle of precipitation is evident

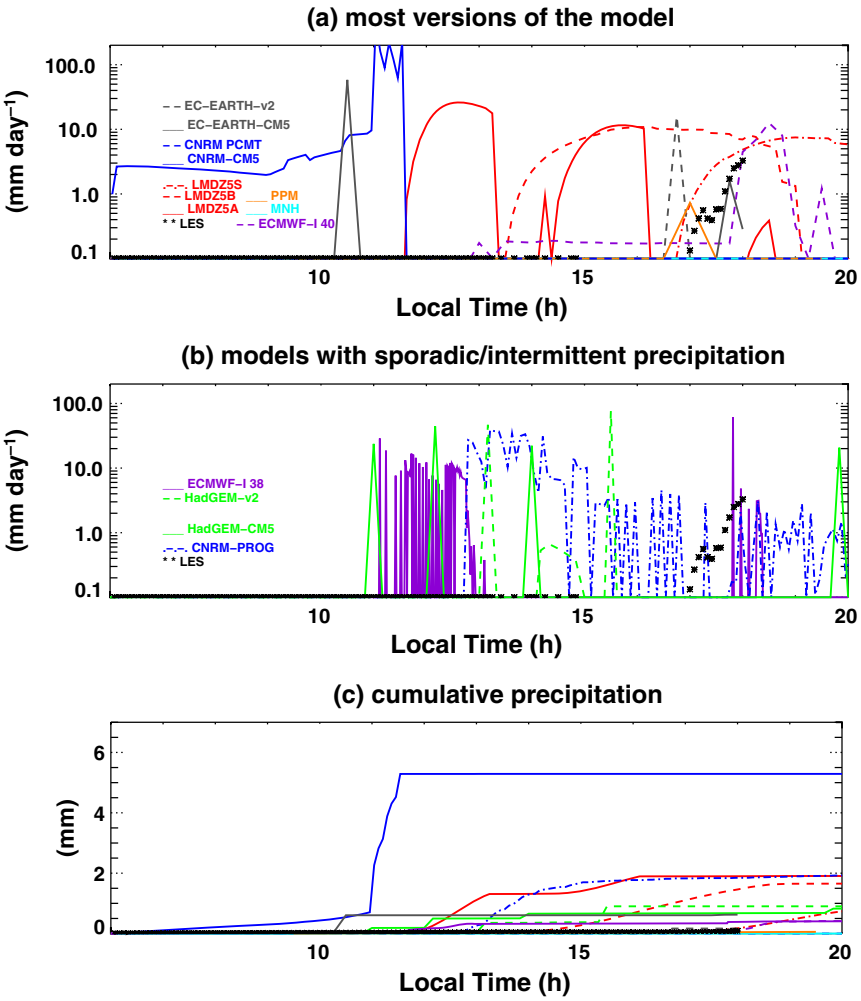

Figure 2. Time evolution of instantaneous precipitation (in mm day^{-1} with a logarithmic axis) for (a) most of the models, (b) the versions of the model that tend to switch on and off the convection scheme and (c) cumulative precipitation (in mm) for the LES (black stars) and the different SCM simulations (in colour).

for several models, and in particular all versions used in the CMIP5: the CNRM-CM5, with a too large precipitation amount after 1000 UTC (previously the precipitation was due mainly to the large-scale scheme), and the LMDZ5A, HadGEM-CM5, ECMWF-I38 and EC-Earth-CM5, with onset of deep convection roughly in phase with the surface flux maximum. The initiation of deep convection is associated with a warming of the levels below 10 km around noon (Figure 3). In agreement with the excessive precipitation amount, the warming is excessive in the CNRM-CM5 and also in the ECMWF-I38 and the EC-Earth-CM5 to a lesser extent. Similarities between the EC-Earth-CM5 and ECMWF-I38 are consistent with their very close physics packages.

Most models predict accumulated precipitation ranging from 1 to 2 mm, but up to 5 mm for the CNRM-CM5, as shown by Figure 2(c), and simulate too early onset, except the EC-Earth-v2, LMDZ5S, ECMWF-I40, MNH, PPM and CNRM-PCMT, as shown previously. Some models, such as the ECMWF-I38, HadGEM-CM5 and HadGEM-v2 and CNRM-PROG, exhibit a chaotic behaviour, as highlighted in the surface precipitation time series (Figure 2(b)); this is also visible in the liquid potential temperature and total water tendencies (in particular for the MNH, Figures 3 and 4). This occurs when the parametrization of deep convection is activated and then rapidly switched off, as highlighted in G04 and also noted in three-dimensional outputs available from the CMIP5 runs (not shown); this behaviour is not an artefact of the one-dimensional set-up.

The total water-mixing ratio tendency (Figure 4) varies from one model to another, with a dipole structure for the ECMWF-I38, ECMWF-I40, EC-Earth-CM5, EC-Earth-v2, MNH and CNRM-CM5 characterized by a moistening in the upper levels (above 5 km), and a drying in the mid-levels (between 2 and 5 km). In the CNRM-PCMT and PPM congestus are initiated at around 1530 UTC, and the associated convective transport of temperature and moisture is consistent with the LES, but the CNRM-PCMT does not really initiate deep convection.

A common feature of the more recent parametrizations is to delay the triggering of precipitation compared with previous model versions. In Figure 3, the timing of initiation of deep convection, determined by the time at which a significant warming of the levels between 6 and 12 km occurs, is indicated by the vertical blue dashed line. For example, the onset is shifted from 1135 to 1315 UTC from the LMDZ5A to LMDZ5B and to 1550 for the LMDZ5S, from 1045 to 1700 from the EC_Earth-CM5 to EC-Earth-v2, from 0940 to 1250 from the CNRM-CM5 to CNRM-PROG, from 1040 to 1255 from the HadGEM-CM5 to HadGEM-v2, from 1105 to 1820 from the ECMWF-I38 to ECMWF-I40. In particular, the change of the boundary-layer scheme and the triggering of the deep convection leads to a delay of deep convection and a better simulation of the transport of heat before initiation in the LMDZ5B (*vs.* LMDZ5A) and in the CNRM-PROG (*vs.* CNRM-CM5). The modification of the triggering in the LMDZ5S (*vs.* LMDZ5B) also delays, by almost 3 h, the initiation of deep convection and predicts a correct timing, cooling/warming and magnitude of precipitation. The LMDZ5S also predicts a later (in comparison with the LMDZ5B) subsequent cooling from the cold pools (even though still too intense), which is in better agreement with the LES. The modification of the closure in ECMWF-I40 (*vs.* ECMWF-I38) improves the representation of the diurnal cycle of precipitation and the associated drying/warming. Modification of entrainment rates also strongly affects the time of initiation of convection, as illustrated by the differences between the EC-Earth-CM5 and EC-Earth-v2.

For the ECMWF-I40 precipitation occurs earlier than the onset of significant modification of the temperature at upper levels. This

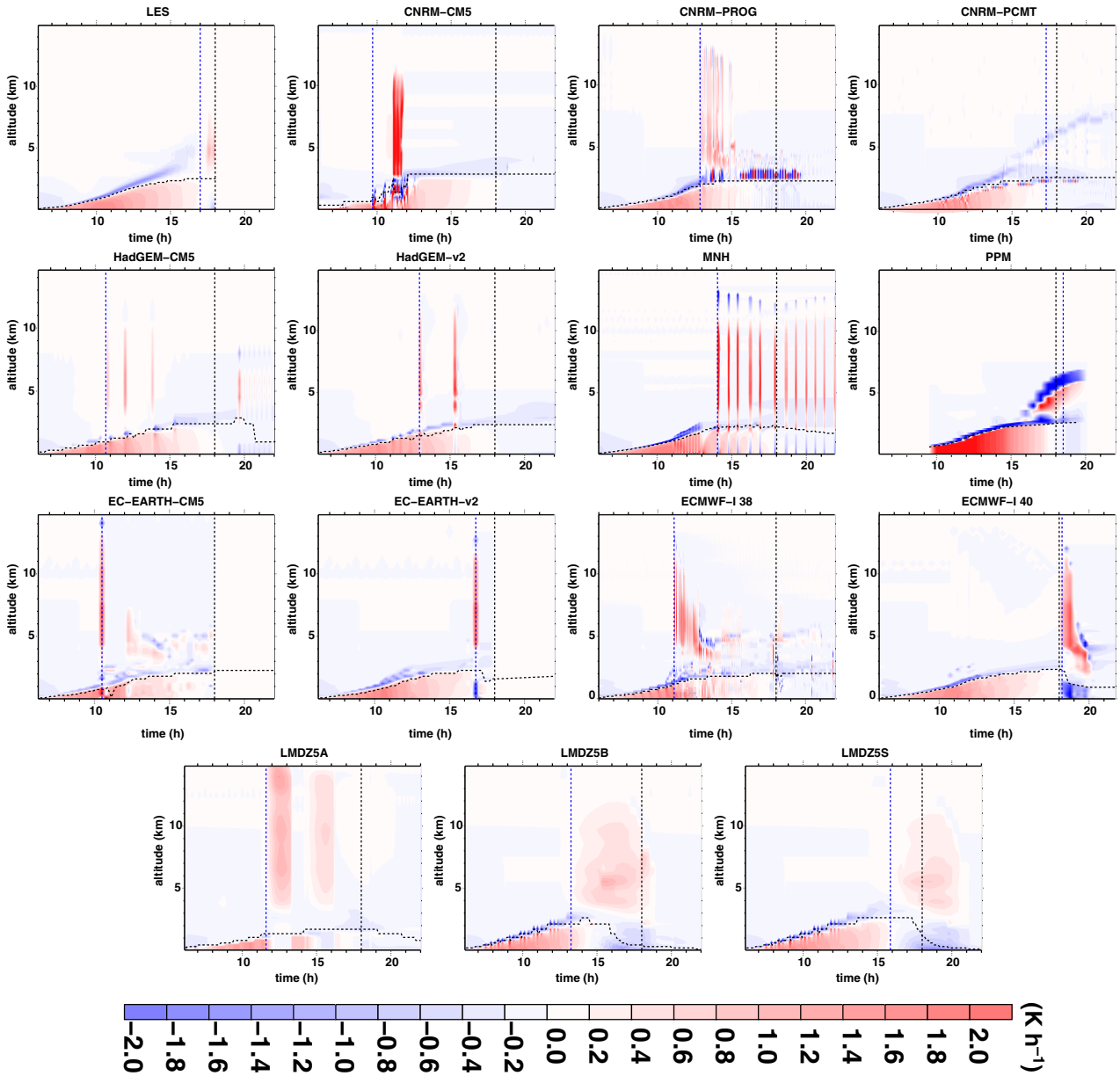

Figure 3. Time evolution of the vertical profiles of the tendency of liquid potential temperature for the LES (upper left) and the different SCM simulations. This is computed and plotted at each model time step. The vertical dashed blue line indicates the time of initiation of the deep convection scheme (detected by a significant warming in the 6–12 km layer) for each SCM simulation. The vertical dashed black line indicates the end of the LES. The boundary-layer height, derived as the level where the integrated virtual potential temperature becomes greater than the average value of the levels below plus 0.25, is shown with a dashed black line.

implies that in those models, even though the triggering condition is achieved, the closure inhibits the impact of the deep convection for some time. This underlines the competing influences of the triggering and closure formulations.

To summarize, there is a large spread among models in terms of timing of convective initiation and intensity of precipitation for this case representative of semi-arid conditions. In general, deep convection occurs too early. The new model developments that concern the triggering function (e.g. LMDZ5B/LMDZ5S), the closure function (e.g. ECMWF-I38/ECMWF-I40) or the entrainment formulation (e.g. EC-Earth-CM5/EC-Earth-v2) or a combination of the three elements (CNRM-PCMT) lead to a significant improvement of the deep convection initiation. The fact that the modification of one of these three components of a convective parametrization leads to a similar impact highlights the complex interactions of the different elements of a convective parametrization and reflects the different processes at play.

3.3. *Evaluation of the triggering formulation*

In order to evaluate the triggering criteria used in the different parametrizations, we apply them offline, when possible, to various thermodynamic profiles, simulated by the LES or simulated by a given model. This provides the times at which convection parametrization would be active for given thermodynamic mean profiles. For a given SCM model, we can compare three times: (i) the time of activation of convection parametrization for the LES thermodynamic mean profiles; (ii) the time of activation of convection parametrization for the SCM thermodynamic mean profiles; and (iii) the time of significant modification of the mean negative liquid potential temperature (θl) profile by the convection parametrization that integrates both the role of triggering and closure function and was used previously. This allows us to distinguish the deficiencies due to the triggering criteria alone from issues related to the modification of the thermodynamic mean profiles by processes acting before initiation of deep convection, such as turbulence and shallow convection. Figure 5 presents those three times for the LMDZ5A, LMDZ5B, CNRM-CM5 and CNRM-PROG models, for which it was relatively easy to separate the triggering criteria. First, it should be emphasized that none of those new triggering times, when applied to the LES thermodynamic mean profiles, matches the time of initiation of deep convection in the LES, meaning that the triggering conditions are still problematic. The time-lag

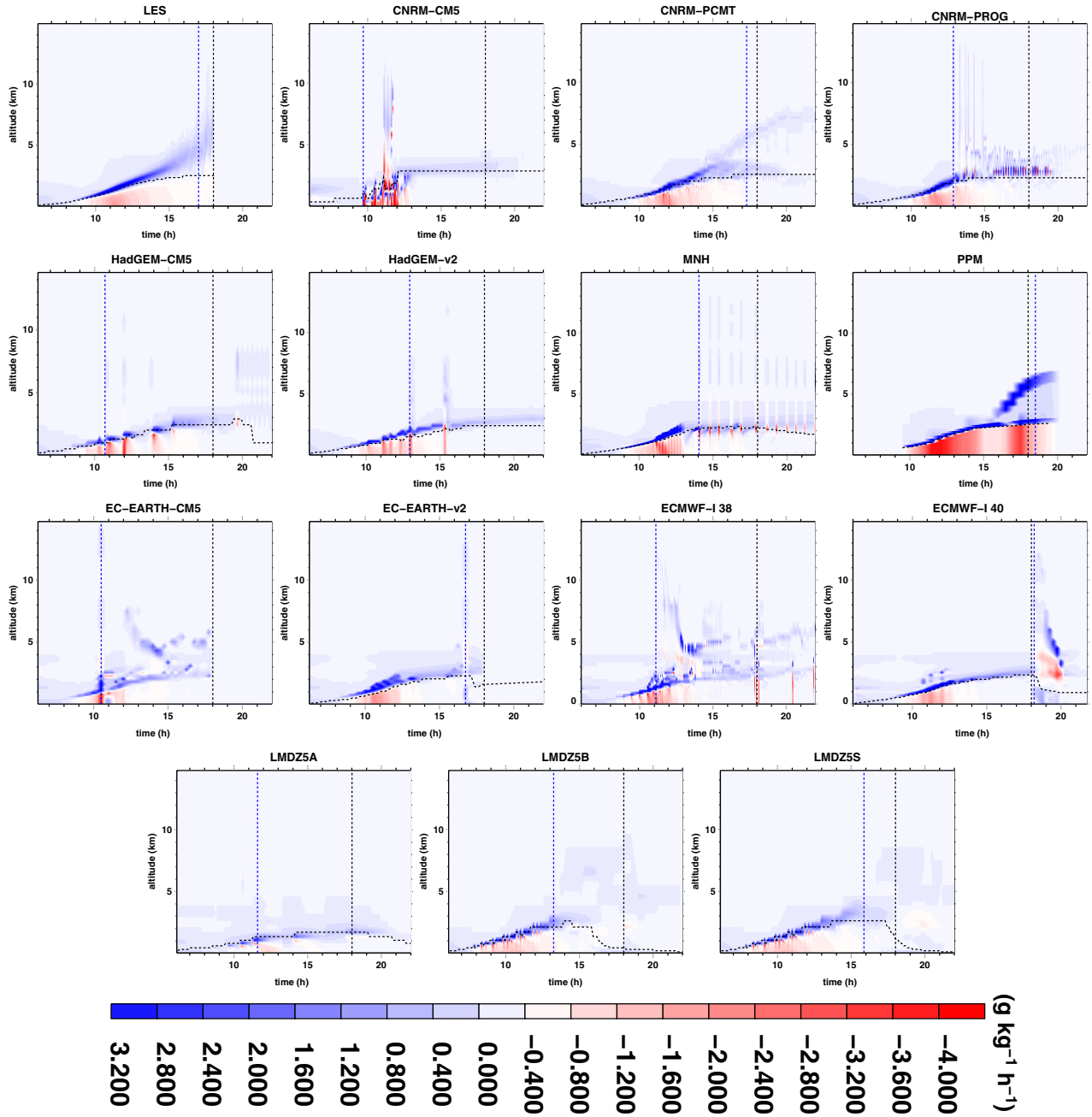

Figure 4. Same as Figure 3 for the tendency of total water mixing ratio.

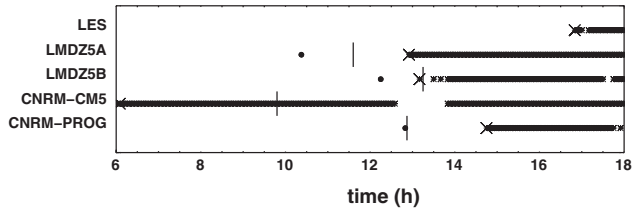

Figure 5. Vertical bars indicate the time of significant warming between 6 and 12 km in the SCMs. Crosses indicate the time of activation of the triggering criteria applied offline to the LES thermodynamic mean profiles: the large cross indicates the first activation time and small crosses the activation time tested for every 5 min profiles. Dots indicate the time of activation of the triggering criteria applied offline to the SCM thermodynamic mean profiles.

between the dot and the cross can be interpreted as the role of the thermodynamic profiles. All triggering criteria except that of the CNRM-CM5 predicts later (1–2.5 h) initiation of convection when using the LES thermodynamic profiles and implies that improved representation of the vertical profiles, mainly in the subcloud layer, may partly correct the simulation of the onset of deep convection. This highlights the role of the boundary-layer processes and shallow convection in the preconditioning of the atmosphere. Note that the difference between the large crosses of the CNRM-CM5 and CNRM-PROG (a delay of 7 h) comes entirely from the addition of a condition on the cloud thickness in the triggering criteria. This suggests that in the CNRM-PROG, the definition of the triggering allows a shallow cumulus to develop because deep convection cannot be activated until clouds (as diagnosed from parcel theory) reach a depth of 3 km. The time-lag between the dots and the vertical bars is related to the impact of the closure, which is significant (from 1 to 4 h) for all models except the CNRM-PROG, meaning that the closure can limit the impact on the mean profiles.

4. Preconditioning of the environment by the boundary layer and shallow clouds

4.1. Representation of the boundary layer and shallow clouds

The SCMs include different representations of boundary-layer turbulence and shallow convection (see Table 1 for details). Six configurations, the CNRM-PCMT, LMDZ5B, EC-Earth (and v2), ECMWF-I (38 and 40) and MNH, use the eddy diffusivity and mass flux concept, which combines a mass-flux scheme that

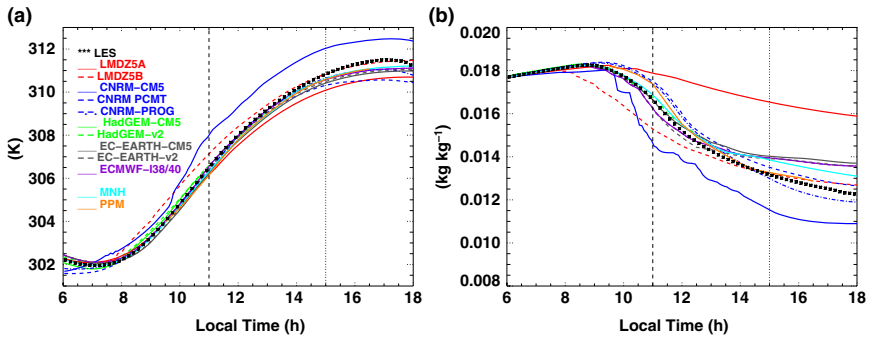

Figure 6. Time evolution of (a) the potential temperature and (b) water-vapour mixing ratio averaged below 500 m for simulations without the deep convective scheme; for the models for which those simulations are not available (HadGEM-CM5, HadGEM-v2 and PPM) information is drawn up to the time of initiation of deep convection. The LES is shown with black stars and the SCM simulations are in colour. The vertical dashed and dash-dotted lines indicate the times at which profiles are drawn in Figures 7 and 8 (11 h) and Figure 11 (15 h) respectively.

represents the effect of coherent structures with a parametrization for the small scale of turbulence based on eddy diffusivity (K-theory or TKE prognostic scheme). Other schemes use either a prognostic (CNRM-PROG) or diagnostic (CNRM-CM5) TKE scheme or a K-mixing theory (with a counter-gradient term for the LMDZ5A, and a non-local mixing length for the HadGEM). We also show results from the PPM, which uses several entraining plume models to represent an ensemble of updraughts initiated from the surface in order to represent the dry or cloudy boundary layer distinguishing the forced (negatively buoyant) and active (positively buoyant) clouds. Only the CNRM-PCMT, LMDZ5B and MNH use the eddy diffusivity and mass flux concept to represent shallow cumulus as well as the boundary layer. Shallow convection schemes in the ECMWF-I (38 and 40), EC-Earth and HadGEM only differ from the deep convection in their entrainment rate and/or closure. In the CNRM-CM5, the shallow convection is represented by the turbulence scheme and associated subgrid condensation scheme.

The entrainment and detrainment formulations used in boundary-layer and/or shallow-convection mass-flux schemes vary from one model to the other. The models handling the shallow convection and the boundary layer separately often use a formulation of the entrainment/detrainment rates similar to the deep-convection scheme for the shallow convection, but sometimes with modified values, for example: in the EC-Earth-CM5, the lateral entrainment rate, which is based on an inverse function of cloud radii, is larger for shallow convection than deep convection; the CNRM-PROG uses a buoyancy-sorting formulation (Bechtold *et al.*, 2001); the LMDZ5B uses the formulation of Rio *et al.* (2010), which relates the entrainment/detrainment formulation to the buoyancy of the updraught, its vertical velocity and water-mixing ratio difference relative to the environment; and the PPM uses a formulation that depends on the boundary-layer height below cloud base and a simplified buoyancy-sorting (De Rooy and Siebesma, 2010) for shallow clouds.

In the following, we evaluate the representation of the thermodynamic vertical profiles before convective initiation, which has been shown to be an important ingredient to deep convective triggering by G04. As shown previously, the early bias of deep convection initiation in the SCMs cools and dries the boundary layer, stabilizes the middle troposphere and therefore inhibits any shallow-convection development. This prevents any further evaluation of the model physics during the preconditioning phase. Therefore, in the following, we focus on additional simulations where the deep convection scheme has been turned off. These have been carried with the LMDZ5A, LMDZ5B (LMDZ5S and LMDZ5B are identical when the deep convection is deactivated, as modifications in LMDZ5S concern only the deep convection scheme), CNRM-CM5, CNRM-PROG, EC-Earth (CM5 and v2) and ECMWF-I (38 and 40 are identical, as the only difference between those two versions is in the deep convection scheme). For the other models, we present results only up to the triggering time.

4.2. *Evolution of the boundary-layer characteristics*

In the LES, the boundary layer is growing up to 2500 m at 1500 UTC, warming by about 8 K and drying by roughly 5 g kg^{-1} from 0600 to 1500 UTC (Figures 3 and 4). The warming is due to the large sensible heat flux and the entrainment of warm air from the layer above during the boundary-layer growth. The drying is due to boundary-layer top entrainment as the latent heat fluxes are weak (Figure 1).

Even though all simulations are performed with the same initial and boundary conditions, large differences rapidly appear among the different models (Figure 6). In particular, an excessively high, warm and dry boundary layer is produced by the CNRM-CM5 and a low, moist and cold boundary layer by the LMDZ5A (after 1000 UTC). In the following, we mainly focus on modifications of those models that lead to improvements.

The modification of the turbulence scheme in the CNRM-PROG (using a prognostic TKE scheme with a non-local mixing length instead of a diagnostic TKE scheme with a local mixing length) improves the representation of the boundary-layer characteristics (mean profiles in Figures 6 and 7 and flux profiles in Figure 8). The CNRM-PROG, however, produces a boundary layer that is too moist (Figures 6(b) and 7(b)) due to the too low moisture flux at the top of the boundary layer (Figure 8(b)). Using a mass-flux scheme in addition to this prognostic TKE scheme, as in the CNRM-PCMT, did not change the results in this case and the moisture flux was still underestimated at the top of the boundary layer. The mass-flux scheme might not have enough impact on the CNRM-PCMT, as shown by a negative gradient of the potential temperature in the whole boundary layer (Figure 7(a)) specific to the absence, or insufficient impact, of the mass-flux scheme.

The deficiency of the LMDZ5A is consistent with the results from Hourdin *et al.* (2002) and is explained by the insufficient transport of heat by the local turbulence scheme (Figure 8). In particular, the LMDZ5A is the only model displaying a non-linear flux profile in the boundary layer although a linear profile is expected. This is improved in the LMDZ5B, via the explicit representation of non-local transport by boundary-layer thermals, in particular after 1400 UTC (Figure 6). The LMDZ5B, however, tends to have excessive boundary-layer growth, leading to a warm and dry bias up to 1300 UTC, which is due to an overly active thermal scheme in the morning, as shown by the overestimated area of positive θl flux (Figure 8(c)). Note that the thermal scheme is less overactive when using a smaller time step of 60 s *versus* 450 s. Concerning the other models, the ECMWF, EC-Earth-CM5 and MNH reproduce boundary layers and vertical transport close to the LES, and the modifications of the physics for the EC-Earth only very slightly modify the boundary layer. The positive gradient of the potential temperature profile in the whole boundary layer for HadGEM-CM5 and v2 (Figure 7) is related to the strong impact of explicit non-local transport terms, consistent with Lenderink *et al.* (2004). By design, as a bulk model, the PPM

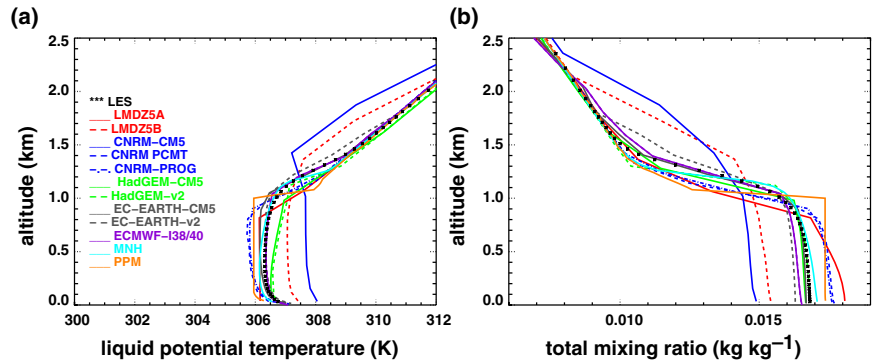

Figure 7. Vertical profile of (a) liquid potential temperature and (b) total mixing ratio at 11 h (just before initiation of shallow clouds in the LES) for simulations without the deep convective scheme. For the models for which those simulations are not available (HadGEM-CM5, HadGEM-v2 and PPM) information is drawn if time of initiation has not been reached.

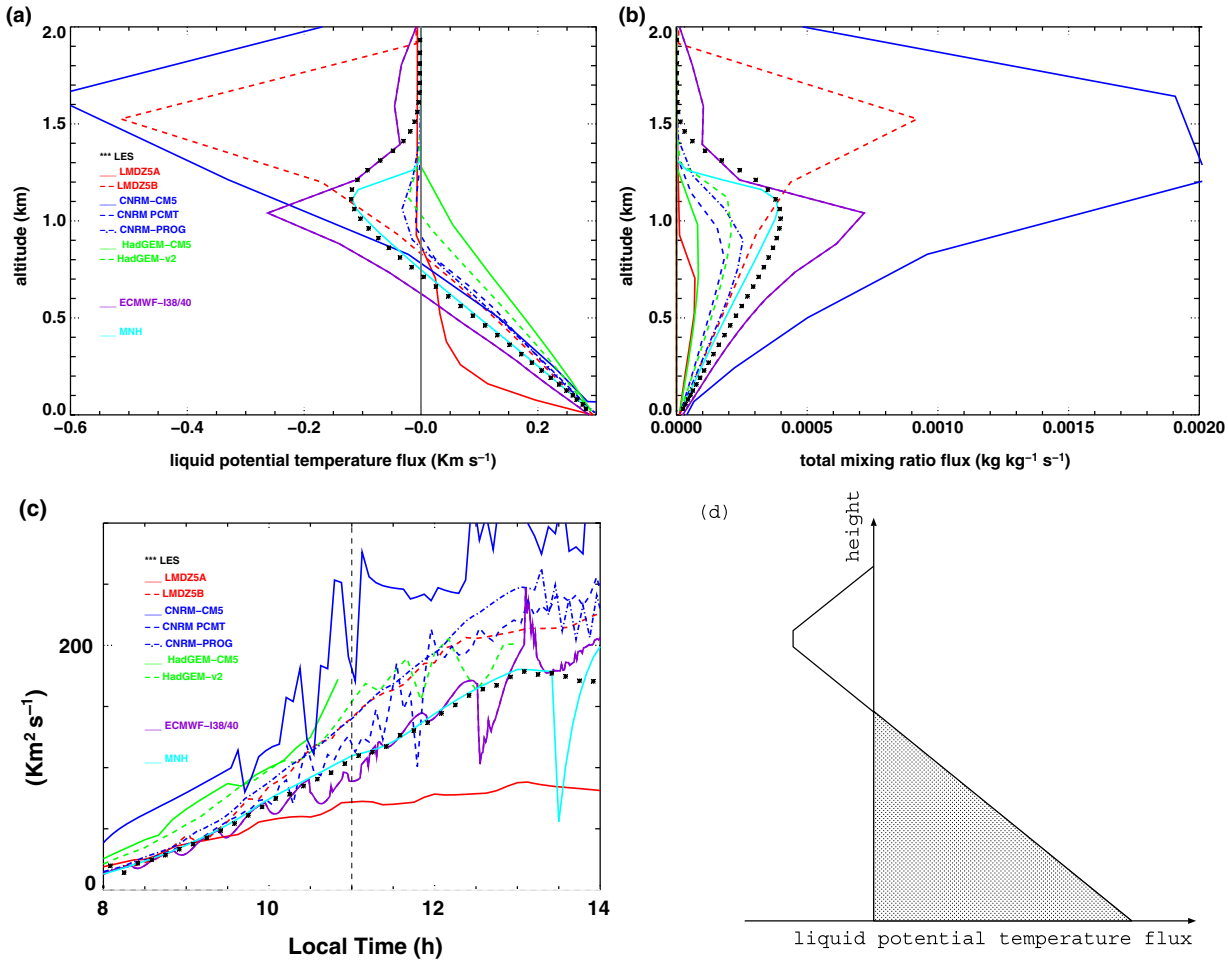

Figure 8. Vertical profile of total (boundary-layer (diffusion plus mass-flux scheme) and shallow convection contribution) fluxes of (a) liquid potential temperature and (b) total mixing ratio at 11 h (just before initiation of shallow clouds in the LES) for simulations without the deep convective scheme. For the models for which those simulations are not available (HadGEM-CM5 and HadGEM-v2) information is drawn as if time of initiation of deep convection has not been reached. For the LES, the subgrid flux plus the resolved flux is drawn. (c) Time evolution of the vertical integral of the positive liquid potential-temperature flux as shown by the dashed zone in the schematic (d). The fluxes were not available for the EC-Earth (both versions) and PPM simulations.

predicts (too) strong jumps at the top of the boundary layer, but the boundary-layer height is well reproduced by this bulk scheme.

To conclude, it seems important to correctly represent non-local transport and top-entrainment in the boundary layer in addition to the small-scale turbulence. In particular, there is a large spread in the intensity of the exchange of air at the top of the boundary layer (illustrated in Figure 8(b)) and this merits further work in the future.

4.3. *Evolution of shallow clouds*

Figure 9 presents the time evolution of the vertical profiles of the cloud condensate for each simulation (all the simulations with the deep convection scheme switched off, and also for the ECMWF-I40 with the deep convection scheme activated, and the PPM) with the LES field interpolated on the same vertical and temporal grids overlaid (blue lines). As detailed in C12 and shown in Figure 9(a), in the LES, the shallow clouds develop around 1030 UTC and deepen progressively, reaching 1 km vertical extent at 1315 and 3 km at 1500 UTC. The models differ in the representation of the shallow convection and the spread across models is large, although it is reduced compared with Lenderink *et al.* (2004). The LMDZ5A strongly underestimates the cloud condensate in terms of cloud depth or content, with no cloud (in the configuration with the deep convection scheme some shallow clouds form immediately after 1520 UTC) at all before 1700 UTC, even though it has a much lower lifting condensation level (LCL)

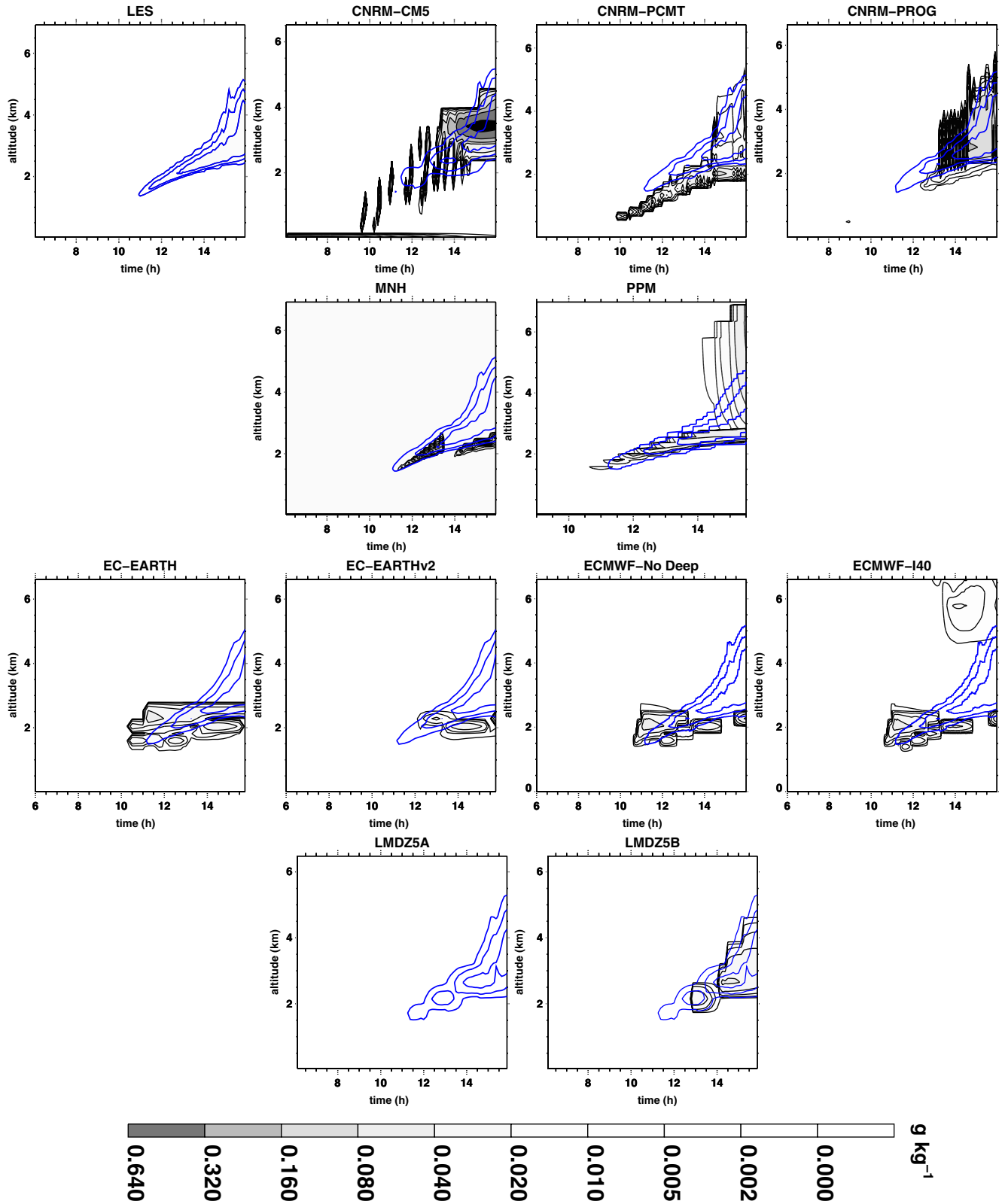

Figure 9. Time evolution of the vertical profiles of the cloud condensate (liquid-water content plus ice-water content) for the LES (upper left) and the different SCM simulations. The LES field interpolated on the vertical and temporal grid of the model is overplotted with contours (same contours as the shading). Only the runs available with the deep convection scheme de-activated are shown except for ECMWF for which, as an illustration, both the results with and without the activation of deep convection are shown.

than the LES (not shown). This is improved in the LMDZ5B due to the representation of shallow clouds by the mass-flux scheme. Some models underestimate the cloud depth, such as the EC-Earth, EC-Earthv2, MNH or ECMWF-I40 (activating deep convection does not really change the production of shallow clouds). Other models tend to initiate shallow clouds too early and with too much cloud condensate, such as the CNRM-CM5 and CNRM-PROG (shallow clouds develop from 0830 to 1030 with very small cloud condensate and then from 1230 UTC). The CNRM-PCMT initiates shallow clouds too early before 1000 UTC but has a correct vertical extension. The CNRM-PCMT and CNRM-PROG have a lower LCL (consistent with the moister boundary layer) than the LES, and the PPM rapidly switches from shallow clouds thinner than 1 km to deep convective clouds at 1400 UTC. Interestingly, the models with unified representation of shallow and deep convection (CNRM-PCMT and PPM) seem to handle the representation of the transition from shallow to deep convection better. One question arises that deserves

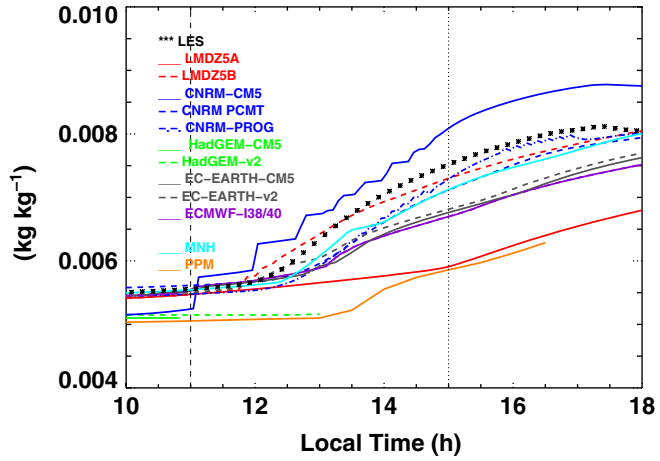

Figure 10. Time evolution of the water-vapour mixing ratio averaged between 2000 and 5000 m for simulations without the deep convective scheme; for the models for which those simulations are not available (HadGEM-CM5, HadGEM-v2 and PPM) information is drawn up to the time of initiation of deep convection. The LES is shown with black stars and the SCM simulations in colour. The vertical dashed and dotted lines indicate the times at which profiles are drawn in Figures 7 and 8 (11 h) and Figure 11 (15 h) respectively.

further investigation is, which scheme (shallow or deep) should represent the congestus phase of the clouds? Even though the spread across the SCMs and LES has been reduced in terms of cloud representation compared with the intercomparison of Lenderink *et al.* (2004), we can conclude from our analysis that the representation of shallow clouds still remains a challenge for models and deserves further work.

In order to quantify the moisture transport by shallow convection the averaged water-vapour mixing ratio between 2 km (level reached by the boundary-layer top around 1300 UTC) and 5 km is shown in Figure 10. Most models underestimate the moistening of this layer, which is consistent with Guichard *et al.* (2004). The LMDZ5A strongly underestimates the moistening, which may explain the absence of shallow clouds, and moistening is also underestimated by the EC-Earth (both versions), ECMWF and PPM. The thermal plume model in the LMDZ5B leads to a better representation of the progressive moistening of the mid-levels, with shallow cumulus clouds present after 1300 UTC, and the MNH, CNRM-PCMT and CNRM-PROG also reproduce the gradual moistening but still underestimate its magnitude. For the LMDZ and CNRM, the new physics greatly improve the moistening by shallow clouds. This is illustrated in Figure 11, which presents the vertical profile of the thermodynamic variables at 1500 UTC. Only the CNRM-PCMT, CNRM-PROG and LMDZ5B reproduce the less stable gradient characteristics of the shallow cumulus layer. The gradual moistening is also visible for those models in the relative humidity profile, with this variable being more directly related to the occurrence of clouds.

All the simulations where the deep convection scheme is active switch rapidly from thin, shallow, cumulus clouds to deep convective clouds, and therefore have difficulties in representing the relatively long-lasting shallow cumulus/congestus phase of this case and the associated humidification of the mid-levels. The incorrect congestus phase in SCMs is related to the triggering of deep convection, which inhibits further development of shallow clouds, but as highlighted above, simulation of the shallow clouds is also an issue for this case in terms of cloud condensate and moistening of the environment by shallow clouds.

5. Influence of the initial and boundary conditions on the timing of convective initiation

Timing of convective triggering was shown in C12 to be sensitive to the initial and boundary (surface fluxes and large-scale advection) conditions. Hereafter we assess whether these sensitivities are captured by the SCMs. Those tests have been carried out by the CNRM for the three physics packages, and by the LMDZ5B, the two versions of the EC-Earth and by the ECMWF-I40.

5.1. *What drives convective initiation in the LES?*

Table A1 summarizes all the sensitivity tests that have been performed to analyse the sensitivity of convective initiation to initial and boundary conditions: significant variations in the initial profiles of the water-vapour mixing ratio, potential temperature (various lapse rates below 5 km) and wind speed, in both horizontal large-scale advection and large-scale vertical velocity. These sensitivity tests have also been performed with the LES. As shown in Figure 12, the sensitivity of the LES can be summarized as follows (see also C12 for more details).

1. Moister initial profiles (whatever the levels: basp, midp, higp) induce an earlier initiation of deep convection, with the largest impact (slightly more than 1 h) at mid-levels (i.e. 750–3000 m); this is probably related to the fact that this test leads to more integrated water vapour than that at low levels.
2. A smaller lapse rate (stabm) induces an earlier (2.5 h earlier) initiation of both shallow and deep convection, more precipitation and cloud fraction and a shorter transition from shallow to deep convection consistent with theoretical understanding (Gentine *et al.*, 2013a).
3. Deep convection is very sensitive to the large-scale vertical velocity (w0–w3) with stronger large-scale vertical velocity (w2 and w3) leading to earlier deep convection and more precipitation and vice versa, which is consistent with previous studies on deep convection, but the coupling between large-scale vertical velocity and deep convection is analysed here at smaller time scales.
4. Very weak sensitivity to the change in horizontal advection (both temperature and moisture: noadv);

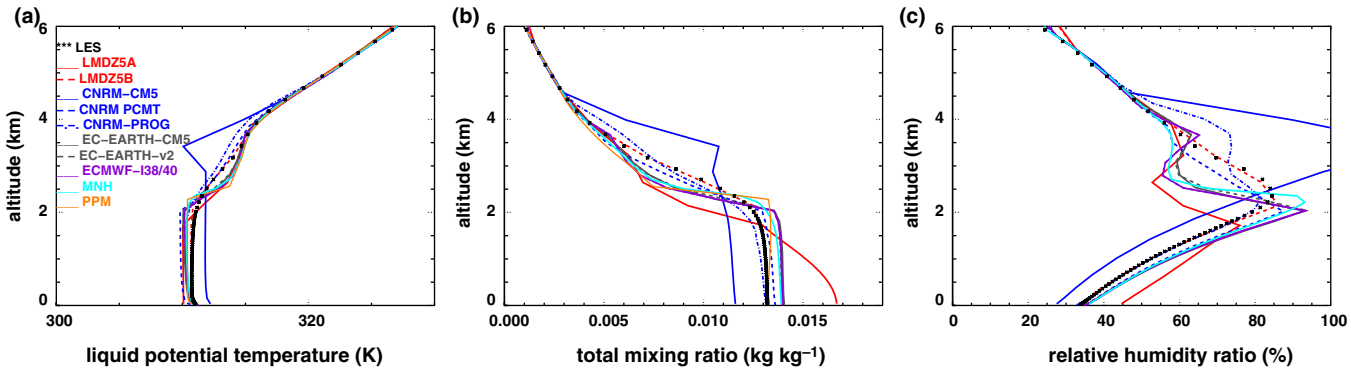

Figure 11. Vertical profile of (a) liquid potential temperature, (b) total mixing ratio and (c) relative humidity at 15 h (time of shallow cumulus development in the LES) for simulations without the deep convective scheme.

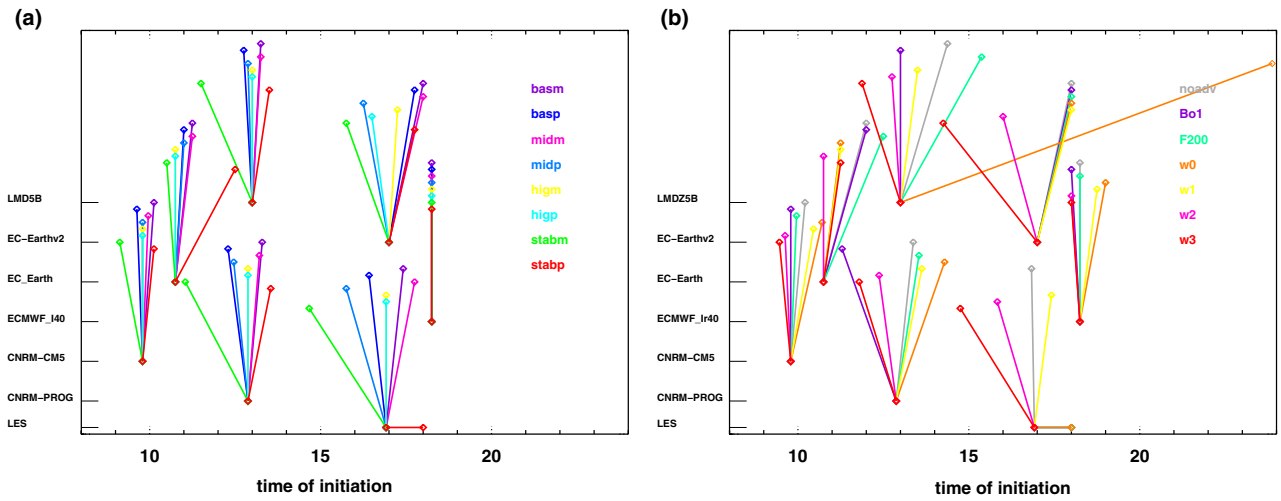

Figure 12. Modification of the time of initiation of convection (defined as the time of significant warming in the upper layer; see text) as a function of the different sensitivity tests to (a) initial conditions of the simulations and (b) boundary conditions. Note that the *y*-axis has no meaning and has been chosen only in order to be sure that all bars are visible. Note that a vertical bar denotes that there is no change in the initiation time of deep convection from the reference time.

5. Lower sensible heat fluxes (F200 and Bo1) prevent any initiation of convection. So, the case needs a relatively large sensible heat flux in order to initiate deep convection. This allows a high enough boundary layer to reach the lifting condensation level and generate convection, similar to the idea of negative surface-moisture–precipitation feedback pertaining to deep boundary layers (Guichard *et al.*, 2009).

To sum up, the LES is very sensitive to modification of the initial moisture profile and initial stability, as well as to the intensity of the sensible heat flux and strength of the large-scale vertical velocity.

5.2. *Sensitivity to the initial profiles*

All models reproduce the variation of boundary-layer characteristics among the various sensitivity tests to initial profiles simulated by the LES (not shown). Concerning the variations in terms of the initiation of deep convection, as shown in Figure 12(a), all models except the ECMWF-I40 reproduce the sensitivity to the stability, with an earlier initiation for the less stable initial profile (stabm) and a later initiation for the more stable initial profile (stabp), but with a smaller sensitivity than the LES. Similarly, most models, except the ECMWF-I40, reproduce the sensitivity to the moisture, with an earlier initiation for moister low or mid-levels (basp and midp, except the EC-Earth-CM5 for the low levels) and later initiation for drier low and mid-levels (basm and midm), but with a variety in the strength of response. Those tests led to a range of 3.5 h for the LES against 0.5 h for the CNRM-CM5, 2 h for the LMDZ5B, 2.5 h for the CNRM-PROG and 3 h for the EC-Earth (CM5 and v2). In the ECMWF-I40, no variability among those tests is seen in terms of timing of initiation, however, variability in terms of precipitation intensity and boundary-layer characteristics is produced (not shown). Less sensitivity to the moisture at higher levels is noted in both the LES and SCMs.

5.3. *Sensitivity to the boundary conditions*

All the models reproduce a similar sensitivity of boundary-layer characteristics to the imposed boundary conditions as the LES (not shown). The response of the SCMs to the boundary conditions for initiation of deep convection (Figure 12(b)) is more varied than the response to the initial conditions. The EC-Earth presents a different sensitivity, with a delay of initiation for higher large-scale vertical velocity (w2 and w3). Other models do represent the main sensitivity to large-scale velocity; in particular, the LMDZ5B shows a delay for the case with no large-scale vertical velocity, similar to the LES. Most of the models (except the ECMWF-I40) are sensitive to the change in large-scale horizontal advection (noadv), with a delay of initiation in the absence of advection, which is not the case for the LES.

The EC-Earth-CM5 and EC-Earth-v2 are the only models that delay convective initiation for both flux tests. The sensitivity is nonetheless smaller than in the LES. The LMDZ5B is sensitive only to the total amount of energy (F200) and does not show distinctive behaviour for different partitions of the energy into latent and sensible heat fluxes: the time of initiation is not modified when the Bowen ratio is varied (Bo1). The CNRM-CM5 and ECMWF-I40 exhibit almost no sensitivity to the change in surface fluxes and the CNRM-PROG shows an earlier initiation of convection associated with more surface latent heat fluxes (Bo1), as well as different boundary-layer characteristics correctly reproduced by the SCM models with cooler and moister air (not shown). So, none of the models reproduce the strong sensitivity to surface fluxes simulated by the LES even though they produce consistent modifications of the boundary-layer characteristics. This result suggests that the connection between the surface fluxes and the boundary-layer parametrization is correctly reproduced, but not its influence on the initiation of deep convection. This might also be relevant to the finding of Taylor *et al.* (2012) that all the CMIP5 models and the reanalysis tended to trigger deep convection over moister soil, whereas observations indicate a tendency to trigger deep convection over drier soil, in particular in semi-arid regions.

In summary, the models and the LES display similar sensitivities to the initial and boundary conditions in terms of boundary-layer characteristics, but the models fail to reproduce the sensitivity of initiation of deep convection to the boundary conditions in particular large-scale vertical velocity and surface fluxes. This highlights the need to improve the physics of triggering criteria used in those models.

6. Conclusions and perspectives

This study focuses on evaluation of the modelling of daytime convection in semi-arid conditions with the turbulent and convective parametrizations currently used by different weather forecast and climate models, notably the models that participated in the CMIP5 intercomparison. We also assessed the improvements achieved with recent developments in these parametrizations. The proposed set-up is simple but realistic, with well-constrained initial and boundary conditions. It allowed us to investigate the behaviour of parametrizations in environmental conditions that have only barely been explored. This specific case of semi-arid environments differs from other intercomparison studies in showing strong growth of the boundary layer, driven by large surface sensible-heat fluxes, a long-lasting shallow cumulus

phase and late convective initiation, with little precipitation. This case proves to be a valuable test for evaluating the representation of turbulence, shallow and deep convection, as well as the transition from one regime to the other.

In order to provide an in-depth evaluation of the representation of the boundary layer and shallow cumulus, additional simulations with the deep convection scheme switched off were analysed. Despite the relatively constrained set-up (same initial and boundary conditions and no deep convection activated), relatively large differences in boundary-layer characteristics among the different SCMs appear, due to either a misrepresentation of the boundary-layer height or a misrepresentation of the entrainment process at the top of the boundary layer. The explicit representation of non-local transport via a mass-flux parametrization or a non-local mixing length improves the representation of the boundary layer.

In most of the SCMs, the shallow cumulus phase is quasi-absent or very short (even with deep convection switched off) and the associated moistening of the mid-levels is underestimated. So, the SCMs struggle to reproduce the long-lasting shallow cumulus phase, probably due to an underestimation of the subcloud-layer and cloud-layer exchanges. The shallow cumulus phase was highlighted as a critical period by G04 and it appears that this has not been improved much since then and still deserves dedicated work. A unified scheme, however, where shallow and deep convection is handled by the same scheme, as in the CNRM-PCMT or PPM, reproduces this phase better. Models also have difficulty in reproducing the clouds in terms of cloud fraction and water content. This has not been strengthened much here because we prevented cloud radiative feedback at the surface, but our results point to the need for further studies of the surface–atmosphere coupled system. For example, the SCMs do not correctly represent the sensitivity of convective initiation to the amount of surface fluxes. Also the role of surface heterogeneities has not been studied here and is left for further study.

Overall, all the CMIP5 versions of the models initiate deep convection too early, as previously found over land in other climatic regions, and most of the time also with an intensity that is too large. For each model, the recent modifications allow a delay in the time of initiation of convection, although often not enough. This has been achieved in different ways: (i) by coupling the boundary layer with the triggering and closure of the deep convection scheme in the LMDZ5B and in the ECMWF_I40; (ii) by modifying the triggering of deep convection to take into account a spectrum of thermal sizes in the LMDZ5S; (iii) by modifying the entrainment and detrainment rates as in the EC-Earth-v2; (iv) by modifying the representation of the boundary layer and shallow cumulus as in the CNRM-PROG. The coupling of the deep convection scheme with information from the low levels was highlighted by one of the first intercomparisons on the diurnal cycle of convection (G04) and seems to have led to significant improvements, in particular in the ECMWF and LMDZ models. We therefore suggest that for the other models, future developments should focus on the triggering of the deep convection and the coupling with the boundary layer. The present study has also highlighted the complexity of the deep-convection scheme and the competing role of the triggering, closure and entrainment/detrainment rate formulations.

In this case, and as frequently observed over semi-arid land, cold pools form and play a role in the maintenance of the deep convection. We plan to analyse the role of cold pools further, focusing on observations, the LES and the LMDZ5B model, which includes an explicit representation of this process.

Acknowledgements

This work was funded by the European Commission's Seventh Framework Programme, under Grant Agreement number 282672, EMBRACE project. We are grateful to Jean-Philippe Lafore for his coordination effort on this project and to the two anonymous reviewers for their helpful comments.

Appendix

Vertical grid and robustness of the results

All the models used have their standard vertical grid, and therefore the vertical grid differs from one model to the other. Figure A1 presents the vertical thickness of each vertical level for the different versions tested in this intercomparison.

Numerous sensitivity tests were carried out in order to assess the robustness of the results. First, a numerical sensitivity test was carried out with all models except the bulk model (which does not have a vertical discretization), using the same prescribed vertical and temporal resolution (the vertical resolution of the HadGEM-v2 model indicated in crosses in Figure A1 with a 60 s time-step). Only minor differences were apparent between those runs and the reference runs; this suggests that the results presented with the standard vertical and temporal resolution of each model are not much dependent on the chosen resolution. The LMDZ5B displays the strongest sensitivity to the time step, with an initiation of convection delay of 1 h.

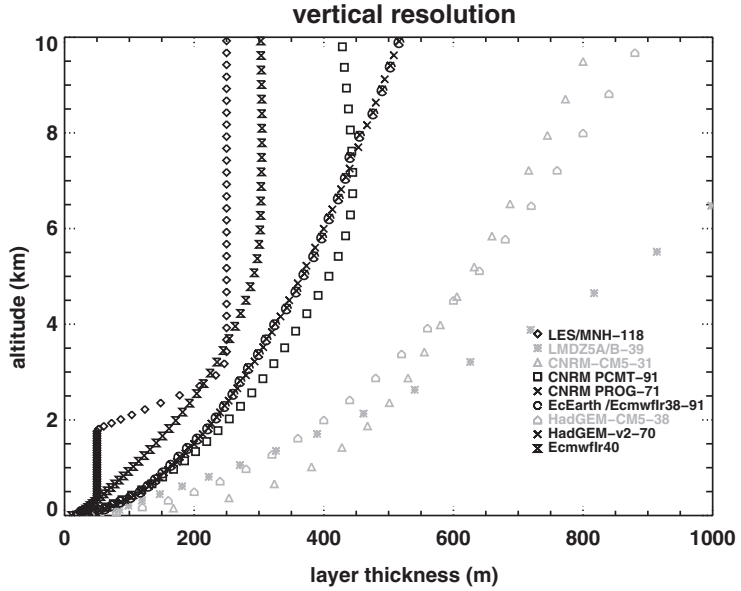

Figure A1. Vertical profile of the vertical thickness of each vertical levels for the different models. Note that only the levels up to 10 km are indicated for clarity.

Table A1. Description of the sensitivity tests.

Name	Maximum of sensible heat flux (W m^{-2})	Maximum of latent heat flux (W m^{-2})	Initial profile of potential temperature (K)	Initial profile of water-vapour mixing ratio (g kg^{-1})	Initial profile of windspeed	Horizontal advection + radiative tendency	Large-scale vertical velocity (cm s^{-1})
Reference	350	50		qv($z = 0$) = 18	AEJ at z ∼4000 m	Yes	1.5
F200	200	–	–	–	–	–	–
Bo1	200	200	–	–	–	–	–
noadv	–	–	–	–	–	No adv	–
w0	–	–	–	–	–	–	0
w1	–	–	–	–	–	–	1
w2	–	–	–	–	–	–	2
w3	–	–	–	–	–	–	3
stabm	–	–	Stability weaker	–	–	–	–
stabp	–	–	Stability stronger	–	–	–	–
basm	–	–	–	Qlow − 0.5	–	–	–
basp	–	–	–	Qlow + 0.5	–	–	–
midm	–	–	–	Qmid − 0.5	–	–	–
midp	–	–	–	Qmid + 0.5	–	–	–
higm	–	–	–	Qhigh − 0.5	–	–	–
higp	–	–	–	Qhigh + 0.5	–	–	–

First column provides the name of the various sensitivity tests used in Section 5. Qxx mean water vapour mixing ratio with xx being low, between the surface and 750 m; mid, between 750 and 3000 m; high, between 3000 and 5000 m.

Table A2. Description of the ensemble runs.

Name	Maximum of sensible heat flux (W m^{-2})	Maximum of latent heat flux (W m^{-2})	Initial profile of potential temperature (K)	Initial profile of water-vapour mixing ratio (g kg^{-1})	Initial profile of wind speed	Horizontal advection + radiative tendency	Large-scale vertical velocity (cm s^{-1})
Reference	350	50		qv($z = 0$) = 18	AEJ at z ∼4000 m	Yes	1.5
Emsemble 1	SHF = 1.1 × SHF_ref	–	–	–	–	–	–
Emsemble 2	–	LHF = 1.1 × LHF_ref	–	–	–	–	–
Emsemble 3	SHF = 0.9 × SHF_ref	–	–	–	–	–	–
Emsemble 4	–	LHF = 0.9 × LHF_ref	–	–	–	-	–
Emsemble 5	–	–	–	Qlow_ref - 0.1	–	–	–
Emsemble 6	–	–	–	Qlow_ref + 0.1	–	–	–
Emsemble 7	–	–	–	Qmid_ref - 0.1	–	–	–
Emsemble 8	–	–	–	Qmid_ref + 0.1	–	–	–
Emsemble 9	–	–	–	Qlhigh_ref - 0.1	–	–	–
Emsemble 10	–	–	–	Qlhigh_ref + 0.1	–	–	–
Emsemble 11	–	–	th - 0.25 K (z = 0–1400 m)	–	–	–	–
Emsemble 12	–	–	th +0.25 K (z = 0–1400 m)	–	–	–	–
Emsemble 13	–	–	–	–	–	tend_rad = 1.1 × tend_rad_ref	–
Emsemble 14	–	–	–	–	–	tend_rad = 0.9 × tend_rad_ref	–
Emsemble 15	–	–	–	–	–	adv_q = 1.1 × adv_q_ref	–
Emsemble 16	–	–	–	–	–	adv_q = 0.9 × adv_q_ref	–
Emsemble 17	–	–	–	–	–	adv_T = 1.1 × adv_T_ref	–
Emsemble 18	–	–	–	–	–	adv_T = 0.9 × adv_T_ref	–
Emsemble 19	–	–	–	–	–	–	1.6
Emsemble 20	–	–	–	–	–	–	1.4

Low, between the surface and 750 m; mid, between 750 and 3000 m; high, between 3000 and 5000 m' Qxx_ref, value of the water-vapour mixing ratio of the reference simulation. SHF stands for sensible heat flux, LHF for latent heat flux, th for the potential temperature, tend_rad for the radiative tendency, adv_q for the moisture advection and adv_T for the temperature advection.

In order to investigate this robustness further, ensemble runs have also been carried out, following Davies *et al.* (2013). Table A2 summarizes the different ensemble runs where slight modifications of the initial profiles, the surface fluxes and the large-scale forcing have been alternatively imposed. They have been run for the LMDZ5, CNRM, EC-Earth and ECMWF-I models. For those models, the dispersion among the various ensemble runs for one model is small, which implies that the results presented are not much dependent on small changes in the definition of the set-up (not shown).

References

Agusti-Panareda A, Beljaars A, Ahlgrimm M, Balsamo G, Bock O, Forbes R, Ghelli A, Guichard F, Köhler M, Meynadier R, Morcrette JJ. 2010. The ECMWF reanalysis for the AMMA observational campaign. *Q. J. R. Meteorol. Soc.* **136**: 1457–1472.

Bechtold P, Bazile E, Guichard F, Mascart P, Richard E. 2001. A mass-flux convection scheme for regional and global models. *Q. J. R. Meteorol. Soc.* **127**: 869–886.

Bechtold P, Semane N, Lopez P, Chaboureau J-P, Beljaars A, Bormann N. 2014. Representing equilibrium and non-equilibrium convection in large-scale models. *J. Atmos. Sci.* **71**: 734–753, doi: 10.1175/JAS-D-13-0163.

Betts AK, Jakob C. 2002. Evaluation of the diurnal cycle of precipitation, surface thermodynamics, and surface fluxes in the ECMWF model using LBA data. *J. Geophys. Res. – Atmos.* **107**: 8045, doi: 10. 1029/2001JD000427.

Bony S, Emanuel KA. 2001. A parametrization of cloudiness associated with cumulus convection; evaluation using Toga Coare data. *J. Atmos. Sci.* **58**: 3158–3183.

Bougeault P. 1982. Cloud ensemble relations based on the gamma probability distribution for the higher-order models of the planetary boundary layer. *J. Atmos. Sci.* **39**: 2691–2700.

Bougeault P. 1985. A simple parameterization of the large-scale effects of cumulus convection. *Mon. Weather Rev.* **113**: 2108–2121.

Browning KA, Betts A, Jonas PR, Kershaw R, Manton M, Mason PJ, Miller M, Moncrieff MW, Sundqvist H, Mitchell J, Hobbs PV, Tiedtke M, Tao WK.

1993. The GEWEX Cloud System Study (GCSS). *Bull. Am. Meteorol. Soc.* **74**: 387–399.

Burpee RW. 1974. Characteristics of North African easterly waves during the summers of 1968 and 1969. *J. Atmos. Sci.* **31**: 1556–1570.

Couvreux F, Rio C, Guichard F, Lothon M, Canut G, Bouniol D, Gounou A. 2012. Initiation of daytime local convection in a semi-arid region analyzed with Large-Eddy Simulations and AMMA observations. *Q. J. R. Meteorol. Soc.* **138**: 56–71, doi: 10.1002/aj.903.

Couvreux F, Guichard F, Gounou A, Bouniol D, Peyrillé P, Koehler M. 2014. Modelling of the diurnal cycle in the lower atmosphere: A joint evaluation of four contrasted climates along a surface temperature gradient over land. *Boundary Layer Meteorol.* **150**: 185–214, doi: 10.1007/s10546-013-9862-6.

Cuxart J, Bougeault P, Redelsperger JL. 2000. A turbulence scheme allowing for mesoscale and large-eddy simulations. *Q. J. R. Meteorol. Soc.* **126**: 1–30.

Dai A. 2001. Global precipitation and thunderstorm frequencies. Part II: Diurnal variations. *J. Clim.* **14**: 1112–1128.

Dai A, Trenberth KE. 2004. The diurnal cycle and its depiction in the Community Climate System Model. *J. Clim.* **17**: 930–951.

D'Andrea F, Gentine P, Betts AK, Lintner BR. 2014. Triggering deep convection with a probabilistic plume model. *J. Atmos. Sci.* **71**: 3881–3901, doi: 10.1175/JAS-D-13-0340.1.

Davies L, Jakob C, Cheung K, Del Genio A, Hill A, Hume T, Keane RJ, Komori T, Larson VE, Lin Y, Liu X, Nielsen BJ, Petch J, Plant RS, Singh MS, Shi X, Song X, Wang W, Whitall MA, Wolf A, Xie S. 2013. A single-column model ensemble approach applied to the TWP-ICE experiment. *J. Geophys. Res.* **118**: 1–20, doi: 10.1002/jgrd.50450.

Derbyshire SH, Maidens AV, Milton SF, Stratton RA, Willett MR. 2011. Adaptive detrainment in a convective parameterization. *Q.J. R. Meteorol. Soc.* **137**: 1856–1871.

De Rooy WC, Siebesma P. 2010. Analytical expressions for entrainment and detrainment in cumulus convection. *Q. J. R. Meteorol. Soc.* **136**: 1216–1227.

Dione C, Lothon M, Badiane D, Campistron B, Couvreux F, Guichard F, Sall MS. 2014. Phenomenology of Sahelian convection observed in Niamey during the early monsoon. *Q.J. R. Meteorol. Soc.* **140**: 500–516, doi: 10.1002/qj.2149.

Dufresne JL, Fujols MA, Denvil S, Cambel A, Marti O, Aumont O, Ballanski Y, Bekki S, Bellenger H, Benslila R, Bony S, Bopp L, Braconnot P, Polcher J, Rio C, Terray P. 2013. Climate change projections using the IPSL-CM5 Earth system model: From CMIP3 to CMIP5. *Clim. Dyn.* **40**: 2123–2165, doi: 10.1007/s00382-012-1636-1.

Emanuel KA. 1993. A cumulus representation based on the episodic mixing model: the importance of mixing and microphysics in predicting humidity. *The Representation of Cumulus Convection in Numerical Models of the Atmosphere*, Meteorological Monograph No. 46. American Meteorological Society: Boston, MA, 185–192.

Findell KL, Eltahir EAB. 2003. Atmospheric controls on soil moisture boundary layer interactions. Part I: Framework and development. *J. Hydrometeorol.* **4**: 552–569.

Forbes R, Tompkins AM, Untch A. 2011. *A New Prognostic Bulk Microphysics Scheme for the IFS*, *ECMWF Technical Memorandum* 649. European Centre for Medium-Range Weather Forecasts Reading, Reading, UK.

del Genio AD, Wu J. 2010. The role of entrainment in the diurnal cycle of continental convection. *J. Clim.* **23**: 2722–2738.

Gentine P, Holtslag AAM, D'Andrea F, Ek MB. 2013a. Surface and atmospheric controls on the onset of moist convection over land. *J. Hydrometeorol.* **14**: 1443–1464, doi: 10.1175/JHM-D-12-0137.1.

Gentine P, Betts A, Lintner BR, Findell KL, Van Heerwaarden CC, Tzella A, D'Andrea F. 2013b. A probabilistic bulk model of coupled mixed layer and convection. Part I: Clear-sky case. *J. Atmos. Sci.* **70**: 1543–1556.

Gentine P, Betts A, Lintner BR, Findell KL, Van Heerwaarden CC, Tzella A, D'Andrea F. 2013c. A probabilistic bulk model of coupled mixed layer and convection. Part II: Shallow convection case. *J. Atmos. Sci.* **70**: 1557–1576.

Gounou A, Guichard F, Couvreux F. 2012. Observations of diurnal cycles over a West-African meridional transect: Pre-monsoon and full-monsoon seasons. *Boundary Layer Meteorol.* **144**, doi: 10.1007/s10546-012-9723-8.

Grabowski WW, Bechtold P, Cheng A, Forbes R, Halliwell C, Khairoutdinov M, Lang S, Nasuno T, Petch J, Tao WK, Wong R, Wu X, Xu KM. 2006. Daytime convective development over land: A model intercomparison based on LBA observations. *Q. J. R. Meteorol. Soc.* **132**: 317–344.

Grandpeix JY, Lafore JP. 2010. A density current parameterization coupled to Emanuel's convection scheme. Part I: The models. *J. Atmos. Sci.* **67**: 881–897.

Grant ALM, Brown AR. 1999. A similarity hypothesis for shallow cumulus transports. *Q. J. R. Meteorol. Soc.* **125**: 1913–1936.

Gregory D, Rowntree PR. 1990. A mass-flux convection scheme with representation of cloud ensemble characteristics and stability dependent closure. *Mon. Weather Rev.* **118**: 1483–1506.

Guérémy JF. 2011. A continuous buoyancy based convection scheme: One- and three-dimensional validation. *Tellus A* **63**: 687–706.

Guichard F, Petch C, Redelsperger JL, Bechtold P, Chaboureau JP, Cheinet S, Grabowski W, Grenier H, Jones CG, Köhler M, Piriou JM, Tailleux R, Tomasini M. 2004. Modelling the diurnal cycle of deep precipitating convection over land with cloud-resolving models and single-column models. *Q.J. R. Meteorol. Soc.* **130**: 3139–3172.

Guichard F, Kergoat L, Mougin E, Timouk F, Baup F, Hiernaux P, Lavenu F. 2009. Surface thermodynamics and radiative budget in the Sahelian Gourma: Seasonal and diurnal cycles. *J. Hydrol.* **375**: 161–177.

Hastenrath S. 1995. *Climate Dynamics of the Tropics.* Kluwer: Dordrecht, Netherlands.

Hazeleger W, Severijns C, Semmler T, Ştefănescu S, Yang S, Wang X, Wyser K, Dutra E, Baldasano JM, Bintanja R, Bougeault P, Caballero R, Ekman AML, Christensen JH, van den Hurk B, Jimenez P, Jones C, Kållberg P, Koenigk T, McGrath R, Miranda P, Van Noije T, Palmer T, Parodi JA, Schmith T, Selten F, Storelvmo T, Sterl A, Tapamo H, Vancoppenolle M, Viterbo P, Willén U. 2010. EC-Earth: A seamless Earth system prediction approach in action. *Bull. Am. Meteorol. Soc.* **91**: 1357–1363.

Hourdin F, Couvreux F, Menut L. 2002. Parameterization of the dry convective boundary layer based on a mass flux representation of thermals. *J. Atmos. Sci.* **59**: 1105–1123.

Hourdin F, Grandpeix JY, Rio C, Bony S, Jam A, Cheruy F, Rochetin N, Fairhead L, Idelkadi A, Musat I, Dufresne JL, Lahellec A, Lefebvre MP, Roehrig R. 2013. LMDZ5B: The atmospheric component of the IPSL climate model with revisited parameterizations for clouds and convection. *Clim. Dyn.*, doi: 10.1007/s00382-012-1343-y.

Jam A, Hourdin F, Rio C, Couvreux F. 2013. Resolved versus parametrized boundary-layer plumes. Part III: Derivation of a statistical scheme for cumulus clouds. *Boundary Layer Meteorol.* **147**: 421–441, doi: 10.1007/s10546-012-9789-3.

Jones CD, Hughes JK, Bellouin N, Hardiman SC, Jones GS, Knight J, Liddicoat S, O'Connor FM, Andres RJ, Bell C, Boo K-O, Bozzo A, Butchart N, Cadule P, Corbin KD, Doutriaux-Boucher M, Friedlingstein P, Gornall J, Gray L, Halloran PR, Hurtt G, Ingram WJ, Lamarque J-F, Law RM, Meinshausen M, Osprey S, Palin EJ, Parsons Chini L, Raddatz T, Sanderson MG, Sellar AA, Schurer A, Valdes P, Wood N, Woodward S, Yoshioka M, Zerroukat M. 2011. The HadGEM2-ES implementation of CMIP5 centennial simulations. *Geosci. Model Dev. Discuss.* **4**: 689–763, doi: 10.5194/gmdd-4-689-2011.

Khairoutdinov M, Randall D. 2006. High-resolution simulation of shallow-to-deep convection transition over land. *J. Atmos. Sci.* **63**: 3421–3436.

Koehler M, Ahlgrimm M, Beljaars A. 2010. Unified treatment of dry convective and stratocumulus-topped boundary layer in the ECMWF model. *Q.J. R. Meteorol. Soc.* **137**: 43–57.

Lafore JP, Stein J, Asencio N, Bougeault P, Ducrocq V, Duron J, Fischer C, Hreil P, Mascart P, Masson V, Pinty JP, Redelsperger JL, Richard E, Vil-Guerau de Arellano J. 1998. The meso-NH atmospheric simulation system. Part 1: Adiabatic formulation and control simulations. *Ann. Geophys.* **16**: 90–109.

Lenderink G, Holtslag M. 2004. An updated length-scale formulation for turbulent mixing in clear and cloudy boundary layers. *Q. J. R. Meteorol. Soc.* **130**: 3405–3427.

Lenderink G, Siebesma AP, Cheinet S, Irons S, Jones CG, Marquet P, Muller F, Olmeda D, Calvo J, Sanchez E, Soares PMM. 2004. The diurnal cycle of shallow cumulus clouds over land: A single-column model intercomparison study. *Q. J. R. Meteorol. Soc.* **130**: 3339–3364.

Lothon M, Saïd F, Lohou F, Campistron B. 2008. Diurnal cycle of the low troposphere of West Africa and impact on the transport of water vapour. *Mon. Weather Rev.* **136**: 3477–3500.

Lothon M, Campistron B, Chong M, Couvreux F, Guichard F, Rio C, Williams E. 2011. Life cycle of a mesoscale circular gust front observed by a C-band radar in West Africa. *Mon. Weather Rev.* **139**: 1370–1388.

Lopez P. 2002. Implementation and validation of a new prognostic large-scale cloud and precipitation scheme for climate and data-assimilation purposes. *Q.J.R. Meteorol. Soc.* **128**: 229–257.

Martin GM, Milton SF, Senior CA, Brooks ME, Ineson S, Reicher T, Kim J. 2011. The HadGEM2 family of Met Office Unified Model climate configurations. *Geosci. Model Devel.* **4**: 723–757.

Medeiros B, Hall A, Stevens B. 2005. What controls the mean depth of the PBL. *J. Clim.* **18**: 3157–3172.

Nesbitt SW, Zipser EJ. 2003. The diurnal cycle of rainfall and convective intensity according to three years of TRMM measurements. *J. Clim.* **16**: 1456–1475.

Nikulin G, Jones C, Giorgi F, Asrar G, Buchner M, Cerezo-Mota R, Christensen O, Dequé M, Fernandez J, Haensler A, van Meijgaard E, Samuelsson P, Sylla M, Sushama L. 2012. Precipitation climatology in an ensemble of CORDEX-Africa regional climate simulations. *J. Clim.* **25**: 6057–6078, doi: 10.1175/JCLI-D-11-00375.1.

Pergaud J, Masson V, Malardel S, Couvreux F. 2009. A parameterization of dry thermals and shallow cumuli for mesoscale numerical weather prediction. *Boundary Layer Meteorol.* **132**: 83–106, doi: 10.1007/s10546-009-9388-0.

Pinty JP, Jabouille P. 1998. 'A mixed-phase cloud parameterization for use in mesoscale nonhydrostatic model: Simulations of a squall line and of orographic precipitations'. In *Proceedings of Conference on Cloud Physics*, Everett, WA, USA, August 1999, 217–220.

Piriou JM, Redelsperger JL, Geleyn JF, Lafore JP, Guichard F. 2007. An approach for convective parameterization with memory: Separating microphysics and transport in grid-scale equations. *J. Atmos. Sci.* **64**: 4127–4139.

Randall DA, Xu K, Somerville RJC, Iacobellis S. 1996. Single Column Models and cloud ensemble models as links between observations and climate models. *J. Clim.* **9**: 1683–1697.

Ricard JL, Royer JF. 1993. A statistical cloud scheme for use in an AGCM. *Ann. Geophys.* **11**: 1095–1115.

Rio C, Hourdin F. 2008. A thermal plume model for the convective boundary layer: Representation of cumulus clouds. *J. Atmos. Sci.* **65**: 407–425.

Rio C, Hourdin F, Grandpeix JY, Lafore JP. 2009. Shifting the diurnal cycle of parameterized convection. *Geophys. Res. Lett.* **36**: L0780, doi: 10.1029/2008GL036779.

Rio C, Hourdin F, Couvreux F, Jam A. 2010. Resolved versus parametrized boundary-layer plumes. Part II: Continuous formulation of mixing rates for mass-flux schemes. *Boundary Layer Meteorol.* **135**: 469–483, doi: 10.1007/s10546-010-9478-z.

Rio C, Grandpeix J-Y, Hourdin F, Guichard F, Couvreux F, Lafore J-P, Fridlind A, Mrowiec A, Roehrig R, Rochetin N, Lefebvre M-P, Idelkadi A. 2013. Control of deep convection by sub-cloud lifting processes : The ALP closure in the LMDZ5B general circulation model. *Clim. Dyn.* **40**: 2271–2292.

Rochetin N, Couvreux F, Grandpeix JY, Rio C. 2014a. Deep convection triggering by boundary layer thermals. Part 1: LES analysis and stochastic triggering formulation. *J. Atmos. Sci.* **71**: 496–514, doi: 10.1175/JAD-D-12-0336.

Rochetin N, Grandpeix JY, Rio C, Couvreux F. 2014b. Deep convection triggering by boundary layer thermals. Part 2: Stochastic triggering parameterization for the LMDZ GCM. *J. Atmos. Sci.* **71**: 515–538, doi: 10.1175/JAD-D-12-0337.

Roehrig R, Bouniol D, Guichard F, Hourdin F, Redelsperger JL. 2013. The present and future of the West African monsoon: A process-oriented assessment of CMIP5 simulations along the AMMA transect. *J. Clim.* **26**: 6471–6505, doi: 10.1175/JCLI-D-12-00505.1.

Siebesma A, Cuijpers J. 1995. Evaluation of parametric assumptions for shallowcumulus convection. *J. Atmos. Sci.* **52**: 650–666.

Smith RNB. 1990. A scheme for predicting layer clouds and their water content in a general circulation model. *Q. J. R. Meteorol. Soc.* **116**: 435–460.

Song H, Lin W, Lin Y, Wolf AB, Neggers R, Donner LJ, Del Genio AD, Liu Y. 2013. Evaluation of precipitation simulated by seven GCMs against the ARM observations at the SGP site. *J. Clim.* **26**: 5467–5492.

Stirling AJ, Stratton RA. 2012. Entrainment processes in the diurnal cycle of deep convection over land. *Q. J. R. Meteorol. Soc.* **138**: 1135–1149, doi: 10.1002/qj.1868.

Stratton RA, Stirling AJ. 2012. Improving the diurnal cycle of convection in GCMs. *Q. J. R. Meteorol. Soc.* **138**: 1121–1134, doi: 10.1002/qj.991.

Svensson G, Holtslag AAM, Kumar V, Mauritsen T, Steeneveld GJ, Angevine WM, Bazile E, Beljaars A, de Bruijn EIF, Cheng A, Conangla L, Cuxart J, Ek M, Falk MJ, Freedman F, Kitagawa H, Larson VE, Lock A, Mailhot J, Masson V, Park S, Pleim J, Söderberg S, Weng W, Zampieri M. 2011. Evaluation of the diurnal cycle in the atmospheric boundary layer over land as represented by a variety of singlecolumn models: The second GABLS experiment. *Boundary Layer Meteorol.* **140**: 177–206, doi: 10.1007/s10546-011-9611-7.

Taylor CM, Gounou A, Guichard F, Harris P, Ellis RJ, Couvreux F, De Kauwe M. 2011. Frequency of Sahelian storm initiation doubled over mesoscale soil moisture patterns. *Nature Geosci.* **4**: 430–433.

Tiedtke M. 1989. A comprehensive mass flux scheme for cumulus parametrization in large-scale models. *Mon. Weather Rev.* **117**: 1779–1800.

Tiedtke M. 1993. Representation of clouds in large-scale models. *Mon. Weather Rev.* **121**: 3040–4061.

Voldoire A, Sanchez-Gomez E, Salas y Melia D, Decharme B, Cassou C, Senesi S, Valcke S, Beau I, Alais A, Chevallier M, Déqué M, Deshayes J, Douville H, Fernandez E, Madec G, Maisonnave E, Moine MP, Planton S, Saint-Martin D, Szopa S, Tyteca S, Alkama R, Belamari S, Braun A, Coquart L, Chauvin F. 2013. The CNRM-CM5.1 global climate model: Description and basic evaluation. *Clim. Dyn.* **40**: 2091–2121, doi: 10.1007/s00382-011-1259-y.

Wilson DR, Bushell AC, Kerr-Munslow AM, Price JD, Morcrette CJ. 2008. PC2: A prognostic cloud fraction and condensation scheme. I: Scheme description. *Q. J. R. Meteorol. Soc.* **134**: 2093–2107, doi: 10.1002/qj.333.

Yang CY, Slingo J. 2001. The diurnal cycle in the tropics. *Mon. Weather Rev.* **129**: 784–801.

